J. Fluid Mech. (2013), *vol.* 729, *pp.* 180–213. © Cambridge University Press 2013
doi:10.1017/jfm.2013.294

Spin-up of a two-component superfluid: analytic theory in arbitrary geometry

Cornelis A. van Eysden† and A. Melatos

School of Physics, University of Melbourne, Parkville, VIC 3010, Australia

(Received 1 November 2012; revised 31 May 2013; accepted 3 June 2013;
first published online 18 July 2013)

The impulsive spin-up of a two-component superfluid and its container is solved analytically for the first time in arbitrary geometry, generalizing the extensively studied case of single-fluid spin-up. The superfluid is modelled by the Hall–Vinen–Bekarevich–Khalatnikov (HVBK) two-fluid equations, neglecting non-hydrodynamic processes like vortex tension and pinning, which are weak in certain applications (e.g. neutron stars) and confined to boundary layers in the inviscid HVBK component in other applications (e.g. helium II spin-up in smooth-walled containers). Both components of the flow are found to be columnar. The spin-up time depends on the geometry, mutual friction coefficients, B, B', the Ekman number E, and the superfluid density fraction ρ_n. For $B \sim O(1)$, the inviscid component undergoes Ekman pumping due to strong coupling to the viscous component, and the azimuthal velocities are 'locked together' during the spin-up. For $B \lesssim E^{1/2}$, there is no Ekman pumping in the inviscid component and the inviscid azimuthal velocity spins up via mutual friction on a combination of the mutual friction and Ekman time scales. The spin-up process is studied in spheres, cylinders (with co- and counter-rotating lids), and cones, and occurs faster in spheres and cones. Ekman pumping is (anti-) clockwise adjacent to the (lower-) upper-right boundary, and mirrored about the rotation axis. The solution obtained by Reisenegger (*J. Low Temp. Phys.*, vol. 92, 1993, p. 77) between slowly accelerating parallel plates is recovered in the associated limit. The hydrodynamic torque on the container decays dual-exponentially with time in a cylinder but not in a sphere or cone, where it is a superposition of exponentials whose time scales vary with latitude. The torque is a good diagnostic of the flow; e.g. it is steepest initially in a sphere with strong mutual friction.

Key words: complex fluids, quantum fluids

1. Introduction

The evolution of the fluid flow inside a rotating vessel in response to an impulsive increase in the angular velocity of the walls, or spin-up, has been the subject of numerous investigations. In their original analysis of the spin-up of a single-component viscous, incompressible, Navier–Stokes fluid, Greenspan & Howard (1963) identified three phases: boundary layer formation, Ekman pumping, and viscous relaxation including inertial oscillations. They showed that Ekman pumping enables the bulk of the fluid to achieve co-rotation on a time scale much faster than viscous

† Email address for correspondence: ave@unimelb.edu.au

https://doi.org/10.1017/jfm.2013.294 Published online by Cambridge University Press

diffusion, through the formation of boundary layers. Since this original study, the spin-up analysis has been extended in various directions. For flows with a density stratification, it was shown that buoyancy restricts the depth at which the Ekman pumping operates, so that some regions of the interior do not achieve co-rotation except over the viscous diffusion time scale (Pedlosky 1967; Walin 1969). In contrast, if the fluid is also compressible, its buoyancy is reduced, relieving the restrictions imposed by stratification (Abney & Epstein 1996; van Eysden & Melatos 2008). The spin-up of electrically conducting fluids has also received considerable attention, where Alfvén oscillations (Easson 1979) and the role of the magnetic diffusivity in forming Hartman layers (Benton & Loper 1969; Loper 1971) have been studied. For a detailed discussion of these effects, the reader is referred to the review article by Benton & Clark (1974).

Hydrodynamic models have also been developed to study classical problems, involving fluids with multiple components, such as suspensions of particles (Onsager 1931; Ishii & Mishima 1984; Geurst 1988; Drew & Passman 1999). The spin-up of a two-component fluid has been analysed to understand batch centrifugal separation in mixtures; however, only numerical solutions have been obtained (Ungarish 1990; Amberg & Ungarish 1993). Multi-component hydrodynamics has also found applications in astrophysics, where it describes the multi-constituent interior of neutron stars (Mendell 1991*a*; Andersson, Sidery & Comer 2006).

Pioneering attempts to obtain theoretical understanding of the nature of spin-up in *superfluids* such as helium II focused on the interaction between the boundaries and quantized vortices in the superfluid (Campbell & Krasnov 1982; Adams, Cieplak & Glaberson 1985). These studies were merged with the classical Ekman picture by Peradzynski, Filipkowski & Fiszdon (1990), who assumed the Wedemeyer ansatz to model the poloidal flow (Wedemeyer 1964). A rigorous analytical treatment was finally provided by Reisenegger (1993), who solved the vortex-fluid equations of motion of Chandler & Baym (1986) between two infinite, rotating parallel plates accelerating at a slow and constant rate. He showed that, when the mutual friction is strong, as in helium II, and there is no vortex pinning, the viscous and inviscid components spin up on the same, temperature-dependent time scale. Near the superfluid transition temperature, classical Ekman pumping occurs in the viscous component, which subsequently spins up the inviscid component via mutual friction. Near absolute zero, spin-up is initiated by the inviscid component, whose vortex lines are strongly coupled to the viscous component (and hence the walls of the container) in the boundary layer by mutual friction, inducing a secondary flow which transports the vortex lines inwards. In the zero temperature limit, spin-up is facilitated by vortex pinning, where the coefficient of the friction force between the vortices and the container walls controls the spin-up time.

Solving the vortex-fluid equations of motion in non-parallel-plate geometries poses a tougher challenge. Because vortex lines must emerge perpendicular to the surface, there is a region close to the surface where vortex lines are not vertical. In this region the linearized equations of motion do not apply and the complete nonlinear equations of motion must be solved. Even in simple systems such as a steadily rotating superfluid-filled sphere, analytic solutions are extremely difficult to obtain. Numerical solutions to the nonlinear Hall–Vinen–Bekharevich–Khalatnikov (HVBK) vortex-fluid equations of motion in cylindrical Couette geometry have been obtained to investigate the shearing of vortex lines (Barenghi & Jones 1988; Barenghi 1992; Henderson, Barenghi & Jones 1995; Henderson & Barenghi 2000) and the transition from Ekman flow to Taylor vortex flow (Henderson & Barenghi 2004), assuming no pinning in both

https://doi.org/10.1017/jfm.2013.294 Published online by Cambridge University Press

cases. A comprehensive numerical study of the HVBK equations in spherical Couette geometry was conducted in a series of papers (Peralta *et al.* 2005, 2006, 2008) that considered no pinning, perfect pinning, and both the Hall–Vinen and Gorter–Mellink forms of the mutual friction to investigate a range of superfluid instabilities. Other than this work, superfluid flow in non-parallel-plate geometries and the complex vortex-boundary interaction remains relatively unstudied, even experimentally.

In many laboratory experiments involving superfluid spin-up, turbulence is expected to arise. Superfluid or 'quantum' turbulence is substantially more complicated than its classical counterpart, and is the subject of much ongoing theoretical and experimental study; see Vinen & Niemela (2002), Tsubota (2009), Vinen (2010), Paoletti & Lathrop (2011) and Skrbek & Sreenivasan (2012) for reviews. While turbulence in the normal component of a superfluid can take a classical form, turbulence in the superfluid component consists of a randomly oriented tangle of vortex lines. At length scales much larger than the quantum length scale (typically taken to be the mean inter-vortex spacing of the tangle), the turbulence is quasi-classical, dominated by Kolmogorov-like eddies. At length scales closer to the quantum scale, relative motion between the normal fluid and vortex lines becomes significant, and the spectrum is modified by dissipation due to mutual friction. In the zero temperature limit, a Kolmogorov-like spectrum transitions smoothly into an 'ultra-quantum' or 'Vinen' regime at the quantum scale, below which the vortex tangle is random, containing no large eddies. Spin-up and spin-down experiments involving superfluids in the zero-temperature limit have been employed to investigate vortex formation, propagation and annihilation in smooth-walled containers (Eltsov *et al.* 2010) and the decay of quantum turbulence by rapidly decelerating a rotating cube to rest (Walmsley *et al.* 2007).

Previous analytic studies of superfluid spin-up are restricted to simple geometries (e.g. parallel plates, cylinders). In this paper we derive an analytic solution for the Ekman flow in a simply connected container of arbitrary shape, whose angular velocity is an arbitrary but prescribed function of time. By generalizing the theory in this way, we create a tool to analyse a much wider set of experiments than has hitherto been possible. The solution is explored for strong and weak mutual friction, yielding new, exact, spin-up formulas in both regimes as well as the complicated intermediate case. We demonstrate that we recover the results of Reisenegger (1993) in the limit of strong mutual friction, slow acceleration, and horizontal boundaries. Further generalization of the theory to Couette geometries and the inclusion of the viscous back-reaction of the fluid on the container are postponed to a future paper. These matters have received little attention analytically in the literature, yet they are vital elements in the interpretation of spin-up experiments involving multi-component superfluids (see references above) and neutron star interiors (Anderson *et al.* 1978; Link, Epstein & van Riper 1992).

To solve the equations of motion, we neglect the vortex tension and hence the region close to the surface where the vortex lines are not vertical. There are a number of applications in which such an approximation is valid, which are elaborated upon in § 2.2. The first is in neutron stars, where the dynamic viscosity exceeds the vortex tension by twelve orders of magnitude. A self-consistent theory of the coupled spin-up of a two-component superfluid and its container is an essential ingredient for understanding a long-standing question in astrophysics: the phenomenon of pulsar glitches (Lyne, Shemar & Smith 2000; Wang *et al.* 2000). Glitches are tiny, impulsive, randomly timed increases in the spin frequency of a rotation-powered pulsar. Their size distribution is scale-invariant, and their waiting time distribution is Poissonian (Melatos, Peralta & Wyithe 2008), consistent with the hypothesis that they arise from

https://doi.org/10.1017/jfm.2013.294 Published online by Cambridge University Press

a self-organized, collective avalanche process (Anderson & Itoh 1975; Warszawski & Melatos 2013). During a glitch, angular momentum stored in the superfluid core of the neutron star is transferred erratically to the solid crust ($\sim$1 % of the total moment of inertia) (Link *et al.* 1992). The trigger is often ascribed to collective unpinning of quantized superfluid vortices, induced when crust–superfluid differential rotation (and hence the Magnus force) exceeds a threshold (Baym, Epstein & Link 1992; Warszawski, Melatos & Berloff 2012). Vortex unpinning is followed by an exponential relaxation phase, during which crust–superfluid co-rotation is restored by dissipative forces (Baym, Pethick & Pines 1969). The spin-up theory developed in this article is combined with radio telescope observations of glitch relaxation to measure the transport coefficients of bulk nuclear matter at densities $\gtrsim 10^{15}$ g cm^{-3} , the only way at present that such measurements can be made (van Eysden & Melatos 2010). The glitch phenomenon is also targeted as a key driver of gravitational wave astronomy in the strategic roadmap published by the Gravitational Wave International Committee (2012).

A second application is the systematic experiments on the spin-up of helium II in a sphere, performed by the Tsakadze group over a decade (Tsakadze & Tsakadze 1972, 1973, 1974, 1980). Glass and plastic spheres, sometimes coated with powders, were used to investigate systems with both weak and strong pinning. The theory derived in this paper achieves excellent agreement with the Tsakadze data at the 0.5 % level, suggesting that the vortex tension plays a minimal role in superfluid spin-up in smooth-walled containers, a result that is discussed in detail in a companion paper (van Eysden & Melatos 2011) and was foreshadowed by Reisenegger (1993).

The paper is divided into four parts. In § 2 we derive the general solution for spin-up of a two-component superfluid in arbitrary geometry. In § 3 we examine the effect of the mutual friction force on Ekman pumping by considering the strong, intermediate and weak coupling regimes. In § 4 we apply the general theory to a selection of geometries. Finally, in § 5, we compute the torque acting on the container in the scenarios in §§ 3 and 4. The torque is a powerful external diagnostic of the often invisible internal flow in the spin-up experiments and astrophysical applications. In passing, we demonstrate that the solution of Reisenegger (1993) is recovered as a special case for slowly accelerating parallel plates.

2. Two-fluid spin-up in a container of arbitrary shape

2.1. *Governing equations*

When helium II is made to rotate, Landau's (Landau & Lifshitz 1959) homogeneous two-fluid description (comprising viscous and inviscid components) no longer describes the flow dynamics completely. The inviscid component forms an array of singular vortex lines, each with quantized circulation. The combined circulation from these vortices produces a net rotation on macroscopic scales, thus minimizing the free energy, and introduce two extra macroscopic effects not present in Landau's theory: (i) a lift force (Magnus force), stemming from relative motion between the vortex lines and the inviscid component; and (ii) a dissipative drag force, arising because the viscous component scatters off the vortex lines. The description of helium II in the presence of a high-density array of vortex lines is described by the Hall–Vinen–Bekharevich–Khalatnikov (HVBK) equations, in which the inviscid component carries a macroscopic vorticity after smoothly averaging the vortex line dynamics. For an informative introduction to the HVBK equations, the reader is referred to Henderson & Barenghi (2000). A more general set of equations, derived

https://doi.org/10.1017/jfm.2013.294 Published online by Cambridge University Press

by Baym & Chandler (1983) and Chandler & Baym (1986), track the vortex-line motion explicitly, and includes a restoring force due to elastic deformations of the vortex lattice. This is necessary to capture the Tkachenko modes seen in laboratory spin-down experiments, where fluctuations in the angular momentum of the superfluid are the result of small oscillations in the displacement of the vortex array. To keep the problem tractable, we do not consider Tkachenko modes in this paper.

The HVBK equations were re-derived by Hills & Roberts (1977), who presented the complete set of equations in their currently used form. The HVBK equations for an incompressible superfluid in a coordinate system rotating about the z-axis with constant angular velocity Ω are (Hills & Roberts 1977; Henderson & Barenghi 2000; Peralta *et al.* 2008)

$$\frac{\partial \boldsymbol{v}_n^*}{\partial t^*} + \boldsymbol{v}_n^* \cdot \boldsymbol{\nabla}^* \boldsymbol{v}_n^* + 2\Omega \boldsymbol{e}_z \times \boldsymbol{v}_n^* = -\boldsymbol{\nabla}^* p_n^* + \nu_n \nabla^{*2} \boldsymbol{v}_n^* + \frac{\rho_s^*}{\rho} \boldsymbol{F}^*, \tag{2.1}$$

$$\frac{\partial \boldsymbol{v}_s^*}{\partial t^*} + \boldsymbol{v}_s^* \cdot \boldsymbol{\nabla}^* \boldsymbol{v}_s^* + 2\Omega \boldsymbol{e}_z \times \boldsymbol{v}_s^* = -\boldsymbol{\nabla}^* p_s^* - \boldsymbol{T}^* - \frac{\rho_n^*}{\rho} \boldsymbol{F}^*, \tag{2.2}$$

$$\boldsymbol{\nabla}^* \cdot \boldsymbol{v}_n^* = 0, \tag{2.3}$$

$$\boldsymbol{\nabla}^* \cdot \boldsymbol{v}_s^* = 0, \tag{2.4}$$

where $\boldsymbol{v}_{n,s}^*$ are the velocities of the 'normal' (i.e. viscous, subscript n) and 'superfluid' (i.e. inviscid, subscript s) components, ν_n is the kinematic viscosity of the viscous component, and * symbolizes a dimensional variable. The centrifugal acceleration is absorbed into the effective pressures $p_{n,s}^*$. The densities of the two components satisfy

$$\rho_n^* + \rho_s^* = \rho, \tag{2.5}$$

where ρ is the total fluid density. The mutual friction force is given by the Hall–Vinen form for a rectilinear vortex array (cf. the Gorter–Mellink form for an isotropic vortex tangle; Peralta *et al.* 2008)

$$\boldsymbol{F}^* = \tfrac{1}{2} B \hat{\boldsymbol{\omega}}_s \times [\boldsymbol{\omega}_s^* \times (\boldsymbol{v}_n^* - \boldsymbol{v}_s^*) - \boldsymbol{T}^*] + \tfrac{1}{2} B' [\boldsymbol{\omega}_s^* \times (\boldsymbol{v}_n^* - \boldsymbol{v}_s^*) - \boldsymbol{T}^*], \tag{2.6}$$

where

$$\boldsymbol{\omega}_s^* = \boldsymbol{\nabla}^* \times \boldsymbol{v}_s^*, \tag{2.7}$$

is the macroscopic vorticity of the superfluid and $\hat{\boldsymbol{\omega}}_s = \boldsymbol{\omega}_s^*/|\boldsymbol{\omega}_s^*|$ is the vortex line direction, and B and B' are dimensionless mutual friction coefficients whose values in terms of microscopic quantities are given by Barenghi, Donnelly & Vinen (1983). The vortex tension force per unit mass, $\boldsymbol{T}^*$, is written as

$$\boldsymbol{T}^* = \nu_s \boldsymbol{\omega}_s^* \times \left(\boldsymbol{\nabla} \times \hat{\boldsymbol{\omega}}_s \right), \tag{2.8}$$

where the vortex tension parameter ν_s has the dimensions of a kinematic viscosity, but its physical meaning is very different: it controls the oscillation frequency of Kelvin waves excited along vortex lines (Henderson & Barenghi 2000).

We introduce cylindrical coordinates (r^*, ϕ, z^*). The fluid is contained in the region

$$-h_l^*(r^*) \leqslant z^* \leqslant h_u^*(r^*), \tag{2.9}$$

where $h_{u,l}^*(r^*)$ are *arbitrary* functions which describe the (axisymmetric) shape of the upper and lower surfaces. The initial conditions are as follows. For $t^* \leqslant 0$, the viscous and inviscid components rotate rigidly but differentially, with $\boldsymbol{v}_n^* = r^* \epsilon \Omega_{n0}^*$ and $\boldsymbol{v}_s^* = r^* \epsilon \Omega_{s0}^*$ in the rotating frame, where ϵ is the Rossby number. The upper and

https://doi.org/10.1017/jfm.2013.294 Published online by Cambridge University Press

lower boundaries also rotate differentially, with $\boldsymbol{v}_u^* = r^*\epsilon\Omega f_u(t)\boldsymbol{e}_\phi$ and $\boldsymbol{v}_l^* = r^*\epsilon\Omega f_l(t)\boldsymbol{e}_\phi$ respectively. In general $f_u(t)$ and $f_l(t)$ can either be specified (e.g. $f_u(t) = f_l(t) = 1$ for classical spin-up), or they can be determined self-consistently by the viscous torque on the container (to be studied in a future paper). The viscous component must satisfy the usual no-slip and no-penetration conditions at the boundaries, while the inviscid component only satisfies no-penetration.

Following previous authors (Greenspan & Howard 1963; Walin 1969; Abney & Epstein 1996), we define the following dimensionless (un-starred) variables: $\boldsymbol{v}_{n,s}^* = \epsilon\Omega L\boldsymbol{v}_{n,s}$, $t^* = E^{-1/2}\Omega^{-1}\tau$, $p_{n,s}^* = \epsilon\Omega^2 L^2 p_{n,s}$, $\rho_{n,s}^* = \rho\rho_{n,s}$, and $\nabla^* = L^{-1}\nabla$. L is a characteristic length scale of the system, such as the cylinder height or the sphere radius. The Ekman number is defined as

$$E = \frac{\nu_n}{L^2\Omega}. \tag{2.10}$$

Ekman pumping occurs for $E \ll 1$, when the rotational inertia dominates the viscous forces. An impulsive change in the angular velocity of the container produces viscous boundary layers on the upper and lower surfaces on the time scale Ω^{-1}. In the layers, the Coriolis force induces a radial outflow, which is replenished by fluid from the interior. This drives a secondary flow of order $E^{1/2}$, in which vorticity is eventually convected from the boundary layer back into the interior. The spin-up time scale is the time for the secondary flow to complete its circulation, given by $E^{-1/2}\Omega^{-1}$, which is reflected in the above scalings.

Linearizing (2.1) and (2.2) with $\epsilon \ll 1$, we obtain

$$E^{1/2}\frac{\partial \boldsymbol{v}_n}{\partial\tau} + 2\boldsymbol{e}_z \times \boldsymbol{v}_n = -\boldsymbol{\nabla}p_n + E\nabla^2\boldsymbol{v}_n + \rho_s\boldsymbol{F}, \tag{2.11}$$

$$E^{1/2}\frac{\partial \boldsymbol{v}_s}{\partial\tau} + 2\boldsymbol{e}_z \times \boldsymbol{v}_s = -\boldsymbol{\nabla}p_s - \boldsymbol{T} - \rho_n\boldsymbol{F}, \tag{2.12}$$

where the linearized form of the mutual friction force is

$$\boldsymbol{F} = B\boldsymbol{e}_z \times [\boldsymbol{e}_z \times (\boldsymbol{v}_n - \boldsymbol{v}_s) - \boldsymbol{T}] + B'[\boldsymbol{e}_z \times (\boldsymbol{v}_n - \boldsymbol{v}_s) - \boldsymbol{T}]. \tag{2.13}$$

The perturbation to the vortex line direction is orthogonal to the rotation axis, and is given by

$$\hat{\boldsymbol{\omega}}_s = \tfrac{1}{2}(\boldsymbol{\omega}_s - \boldsymbol{e}_z\omega_{sz}), \tag{2.14}$$

where $\boldsymbol{\omega}_s = \boldsymbol{\omega}_s^*/(\epsilon\Omega)$ is the dimensionless vorticity in the rotating frame and $\omega_{sz} = \boldsymbol{e}_z \cdot \boldsymbol{\omega}_s$. The linearized form of (2.8) is

$$\boldsymbol{T} = -E_s\nabla^2(\boldsymbol{e}_z \times \boldsymbol{v}_s) - E_s[\boldsymbol{\nabla}\omega_{sz} - \boldsymbol{e}_z(\boldsymbol{e}_z \cdot \boldsymbol{\nabla})\omega_{sz}], \tag{2.15}$$

where the superfluid Ekman number is defined as

$$E_s = \frac{\nu_s}{L^2\Omega}. \tag{2.16}$$

The vortex tension parameter is given by

$$\nu_s = (\Gamma/4\pi)\ln(b_0/a_0), \tag{2.17}$$

where $\Gamma = 2\pi\hbar/m$ is the quantum of circulation, m is the mass of the bosonic entity forming the condensate (the helium atom in He II, or two neutrons in a neutron superfluid), $\hbar$ is Planck's constant divided by 2π, $b_0 = (\Gamma/2\Omega)^{1/2}$ is the inter-vortex spacing, and a_0 is the vortex core radius. Comparing (2.11) and (2.12) using (2.15)

https://doi.org/10.1017/jfm.2013.294 Published online by Cambridge University Press

indicates that the vortex tension does not behave like the viscosity of the normal fluid component; it is a reactive force similar to the component of the mutual friction multiplied by B', not dissipative like the component of the mutual friction multiplied by B.

When solving (2.11)–(2.12), it is more convenient to work in terms of the total fluid velocity, defined as

$$\boldsymbol{v} = \rho_n \boldsymbol{v}_n + \rho_s \boldsymbol{v}_s. \tag{2.18}$$

Combining (2.18) with (2.3)–(2.4) and (2.11)–(2.12), we obtain

$$E^{1/2}\frac{\partial \boldsymbol{v}}{\partial t} + 2\boldsymbol{e}_z \times \boldsymbol{v} = -\nabla p + \rho_n E \nabla^2 \boldsymbol{v}_n - \rho_s \boldsymbol{T}, \tag{2.19}$$

$$\nabla \cdot \boldsymbol{v} = 0. \tag{2.20}$$

Because the mutual friction does not appear in (2.19), it is convenient to use (2.19) and (2.20) rather than (2.12) and (2.4) and solve for $\boldsymbol{v}$ and $\boldsymbol{v}_n$ rather than $\boldsymbol{v}_n$ and $\boldsymbol{v}_s$. If the superfluid velocity is desired, it can easily be computed using (2.18). In terms of $\boldsymbol{v}$, the mutual friction force is

$$\boldsymbol{F} = \frac{1}{\rho_s}\left\{B\boldsymbol{e}_z \times [\boldsymbol{e}_z \times (\boldsymbol{v}_n - \boldsymbol{v}) - \rho_s \boldsymbol{T}] + B'[\boldsymbol{e}_z \times (\boldsymbol{v}_n - \boldsymbol{v}) - \rho_s \boldsymbol{T}]\right\}. \tag{2.21}$$

Our system of equations therefore comprises (2.3), (2.11), (2.19) and (2.20).

Following Greenspan & Howard (1963), we elect to satisfy the continuity equations (2.3) and (2.20) identically by writing

$$\boldsymbol{v} = v_\phi \boldsymbol{e}_\phi - E^{1/2}\nabla \times \left(\chi \boldsymbol{e}_\phi\right), \tag{2.22}$$

$$\boldsymbol{v}_n = v_{n\phi}\boldsymbol{e}_\phi - E^{1/2}\nabla \times \left(\chi_n \boldsymbol{e}_\phi\right) \tag{2.23}$$

where χ_n and χ are the streamfunctions for the viscous and total poloidal velocities. Substituting (2.22) and (2.23) into (2.11) and (2.19) and eliminating the pressures, we obtain

$$\begin{aligned} E^{1/2}\mathscr{L} v_{n\phi} - \frac{\partial v_{n\phi}}{\partial \tau} - 2\frac{\partial \chi_n}{\partial z} &= -B'\left(\frac{\partial \chi_n}{\partial z} - \frac{\partial \chi}{\partial z}\right) + BE^{-1/2}\left(v_{n\phi} - v_\phi\right) \\ &\quad - B'E_s\mathscr{L}\left(\frac{\partial \chi}{\partial z} - \rho_n \frac{\partial \chi_n}{\partial z}\right) \\ &\quad + BE^{-1/2}E_s\mathscr{L}\left(v_\phi - \rho_n v_{n\phi}\right), \end{aligned} \tag{2.24}$$

$$\begin{aligned} E^{3/2}\mathscr{L}^2\chi_n - E\mathscr{L}\frac{\partial \chi_n}{\partial \tau} + 2\frac{\partial v_{n\phi}}{\partial z} &= B'\left(\frac{\partial v_{n\phi}}{\partial z} - \frac{\partial v_\phi}{\partial z}\right) + E^{1/2}B\left(\frac{\partial^2 \chi_n}{\partial z^2} - \frac{\partial^2 \chi}{\partial z^2}\right) \\ &\quad + B'E_s\mathscr{L}\left(\frac{\partial v_\phi}{\partial z} - \rho_n \frac{\partial v_{n\phi}}{\partial z}\right) \\ &\quad + E^{1/2}BE_s\mathscr{L}\left(\frac{\partial^2 \chi}{\partial z^2} - \rho_n \frac{\partial^2 \chi_n}{\partial z^2}\right), \end{aligned} \tag{2.25}$$

$$\rho_n E^{1/2}\mathscr{L} v_{n\phi} - \frac{\partial v_\phi}{\partial \tau} - 2\frac{\partial \chi}{\partial z} = -E_s\mathscr{L}\left(\frac{\partial \chi}{\partial z} - \rho_n \frac{\partial \chi}{\partial z}\right), \tag{2.26}$$

$$\rho_n E^{3/2}\mathscr{L}^2\chi_n - E\mathscr{L}\frac{\partial \chi}{\partial \tau} + 2\frac{\partial v_\phi}{\partial z} = E_s\mathscr{L}\left(\frac{\partial v_\phi}{\partial z} - \rho_n \frac{\partial v_{n\phi}}{\partial z}\right), \tag{2.27}$$

https://doi.org/10.1017/jfm.2013.294 Published online by Cambridge University Press

where we define the operator

$$\mathscr{L} = \frac{\partial}{\partial r}\frac{1}{r}\frac{\partial}{\partial r}r + \frac{\partial^2}{\partial z^2}. \tag{2.28}$$

Equations (2.24)–(2.27) reduce to (5.1) and (5.2) in Greenspan & Howard (1963) in the limit $\rho_n \to 1$ and $B, B', E_s \to 0$.

Following Greenspan & Howard (1963), we search for a solution by separating the flow into an interior component and a boundary layer correction, such that

$$v_\phi = v_\phi^I + v_\phi^u + v_\phi^l, \tag{2.29}$$

$$\chi = \chi^I + \chi^u + \chi^l. \tag{2.30}$$

The upper and lower boundary layer corrections are denoted by superscripts u and l respectively; they vanish away from the boundary. Similar equations hold for $v_{n\phi}$ and χ_n, with subscripts n added to every term in (2.29) and (2.30). We now proceed by considering the interior flow and the boundary layers separately.

2.2. *Vortex tension*

Vortex tension plays a key role in many observed phenomena in terrestrial superfluids such as helium II. For example, vortex tension affects the circulation pattern and critical Reynolds numbers in superfluid Taylor–Couette flow (Barenghi & Jones 1988; Barenghi 1992; Henderson *et al.* 1995; Henderson & Barenghi 2000). It also governs the propagation of Kelvin waves and the onset of quantum turbulence, which arises when the counter-flow velocity along the vortex lines, $(\boldsymbol{v}_n - \boldsymbol{v}_s)\cdot\hat{\boldsymbol{\Omega}}$, exceeds the critical value $|\boldsymbol{v}_{DG}| = 2(2\Omega\nu_s)^{1/2}$ (Glaberson, Johnson & Ostermeier 1974; Donnelly 2005). In the turbulent state, a fully developed, self-sustaining, reconnecting vortex tangle develops, the subject of much present study (Tsubota *et al.* 2004; Tsubota 2009; Vinen 2010; Paoletti & Lathrop 2011). However, there are many superfluid applications in which the vortex tension does not play a dominant role, either because one has $\nu_s \ll \nu_n$, or because the geometry of the system nullifies the tension throughout most of the flow and confines its operation to boundary layers, which sometimes exert a marginal influence on the dynamics overall. This paper is directed at both the above classes of applications.

To evaluate the importance of the vortex tension in any given application, we must evaluate its characteristic strength relative to other forces, taking the geometry into account. The linearized equations (2.1) and (2.2) require $\boldsymbol{\omega}_s^* \parallel \boldsymbol{e}_z$ to leading order. However, at the boundary the vortex lines must touch the surface at right angles (Baym & Chandler 1983), a contradiction in non-parallel-plate geometries. The thickness of the region close to the surface where vortex lines are not vertical is governed by the vortex line tension, and by analogy with the classic Ekman layer $\delta_n = E^{1/2}L$, one defines a vortex tension penetration depth $\delta_s = E_s^{1/2}L$. The vortex tension is negligible when the size of this region is much smaller than any other length scale in the flow, e.g. $\nu_s/\nu_n = E_s/E \ll 1$. The ratio of the tension force to the mutual friction force ($\nu_s/L^2\Omega = E_s$) must also be small.

One example of an important application where vortex tension can be safely neglected is in the inner crust of a neutron star, where neutrons pair according to BCS theory in a $^1S_0$ state, producing an isotropic superfluid analogous to helium II. In the outer core, the neutrons pair into a triplet $^3P_2$ state, producing an anisotropic superfluid analogous to ^{3}He, while protons ($\sim$5 % of the star) form a $^1S_0$ state. This system

https://doi.org/10.1017/jfm.2013.294 Published online by Cambridge University Press

is described by a multi-component fluid theory analogous to the HVBK equations (Mendell 1991*a*; Glampedakis, Andersson & Samuelsson 2011).

In a typical neutron star rotating at $\Omega = 100$ rad s^{-1} with $a_0 = 1.1 \times 10^{-11}$ cm (Mendell 1991*a*), we find $\nu_s = 3.1 \times 10^{-7}$ m^2 s^{-1}. For a typical star with radius 10^4 m, this gives $E_s = 3.1 \times 10^{-17}$. The shear viscosity in a neutron star is due to electron–electron scattering in the proton–electron plasma, giving $\nu_n = 6.0 \times 10^2$ m^2 s^{-1} (Cutler & Lindblom 1987; Mendell 1991*b*), and hence $E = 6.0 \times 10^{-8}$. Therefore in a neutron star, we find $\nu_s/\nu_n = 5.1 \times 10^{-10}$. Clearly, the vortex tension is negligible.

For laboratory experiments with helium II the situation is different. Using the established values of the the shear viscosity and vortex core parameter published by Donnelly (2012), we find $5.54 \times 10^{-8} < \nu_n < 2.34 \times 10^{-7}$ m^2 s^{-1} and $1.12 \times 10^{-7} < \nu_s < 1.13 \times 10^{-7}$ m^2 s^{-1} for $1.3 < T < 1.6$ K. For a typical experiment at $T = 1.6$ K (Tsakadze & Tsakadze 1980), we find

$$E = 4.6 \times 10^{-5} \left(\frac{\nu_n}{5.5 \times 10^{-8} \text{ Pa s}} \right) \left(\frac{\Omega}{3 \text{ rad s}^{-1}} \right)^{-1} \left(\frac{L}{2 \text{ cm}} \right)^{-2}. \tag{2.31a}$$

$$E_s = 9.3 \times 10^{-5} \left(\frac{\nu_s}{1.1 \times 10^{-7} \text{ Pa s}} \right) \left(\frac{\Omega}{3 \text{ rad s}^{-1}} \right)^{-1} \left(\frac{L}{2 \text{ cm}} \right)^{-2}. \tag{2.31b}$$

Therefore, we obtain $0.5 < E_s/E_n < 6.1$ for $1.3 \text{ K} < T < 2.1$ K in helium II. Because ν_s and ν_n are comparable in helium II, the region where the vortex lines are not parallel to the rotation axis is of approximately the same thickness as the Ekman layer. Hence, strictly speaking, vortex tension must be included.

However, for applications like those targeted in this paper, involving the linear spin-up of superfluids in smooth-walled containers at temperatures below 1.6 K, vortex tension turns out to be a weak effect. The reason is subtle and can be understood theoretically by examining the analytic solution of Reisenegger (1993) for slow Ekman pumping between slowly accelerating plates. In the solution, the tension coefficient ν_s only appears in the inviscid velocity component in the boundary layer (in the combination ν_s/ν_n). The qualitative features of the slow-acceleration problem carry over to the impulsive spin-up problem, just like they do in the classical case (Bondi & Lyttleton 1948). Hence, ν_s does not appear in the solution for the interior flow or the viscous velocity component in the boundary layer. Nor, consequently, does it appear in the spin-up time. This is why the spin-up time calculated by Reisenegger (1993), who kept $\nu_s \neq 0$, is recovered by our analysis in § 4, despite assuming $\nu_s = 0$. Physically, this can be understood by realizing that the vortex lines exert no torque on the container and vice versa because they are not pinned. Thus, vortex tension is neglected not on the basis of scaling but because, during the spin-up of smooth-walled containers, the tension ν_s appears only in the inviscid component boundary layer and therefore does not affect the gross dynamics (e.g. spin-up time). This theoretical result is confirmed by experiments.

In a companion paper (van Eysden & Melatos 2011), the helium II spin-up experiments performed by the Tsakadze group over a decade (Tsakadze & Tsakadze 1972, 1973, 1974, 1980) are analysed theoretically for the first time using the theory in this paper. Excellent agreement at the 0.5 % level is achieved between theory and experiment, even though $\nu_s = 0$ is assumed. Naturally there are other systems (e.g. rough-walled containers) where such excellent agreement should not be expected; the boundary conditions for superfluid helium are still not completely understood, especially in non-parallel-plate geometries (Khalatnikov 1965; Peralta *et al.* 2008).

https://doi.org/10.1017/jfm.2013.294 Published online by Cambridge University Press

Turbulence is also common in helium II. Again, the laminar theory in § 2.1 may not apply. We follow the traditional practice in the hydrodynamical literature (Barenghi & Jones 1988; Barenghi 1992; Henderson *et al.* 1995; Henderson & Barenghi 2000) and neglect it here, but again, this neglect is justified in many systems of interest. To check whether the Glaberson–Donnelly instability is excited in the experiments of Tsakadze & Tsakadze (1980), we note that the counter-flow velocity in Ekman pumping scales as $\epsilon E^{1/2}\Omega L = \epsilon(\nu_n\Omega)^{1/2}$. Therefore, turbulence will occur for

$$\epsilon > 2(2\nu_s/\nu_n)^{1/2}. \tag{2.32}$$

In the Tsakadze experiments, we have $\epsilon \sim 0.15$ and $0.5 < \nu_s/\nu_n < 6.1$ for $1.3\ \mathrm{K} < T < 2.1\ \mathrm{K}$, so that laminar flow is expected. Quasi-classical turbulence (macroscopic Kolmogorov-like eddies) is predicted to occur when

$$Re_\alpha = \frac{2-\rho_n B'}{\rho_n B}, \tag{2.33}$$

which is the ratio of the reactive and dissipative components of the mutual friction force, becomes large (Finne *et al.* 2003; Eltsov *et al.* 2010). Equation (2.33) suggests that this occurs when $\rho_n \to 0$ as $T \to 0$. Classical turbulence can also arise, and the Ekman layer in a Navier–Stokes fluid becomes unstable (Greenspan 1968; Reisenegger 1993), for

$$E < \epsilon^2(56.3 + 58.4\epsilon)^{-2}, \tag{2.34}$$

suggesting that $\epsilon < E^{1/2} \ll 1$ is required for laminar Ekman pumping. Using the data above, we find that turbulence is expected for $T > 1.6\ \mathrm{K}$ (van Eysden & Melatos 2011, 2012). Hence, a window exists where laminar flow is possible in helium II, where good agreement with the Tsakadze & Tsakadze (1980) experiments is obtained. The theory presented here is also applicable to other terrestrial fluids, such as superfluid ^{3}He, where turbulence is suppressed at sufficiently high temperatures, and in rotating dilute-gas Bose–Einstein condensates, where the geometry of the trap is non-cylindrical. These applications are discussed in more detail in a companion paper (van Eysden & Melatos 2012).

Linear HVBK theory requires vortex lines to emerge perpendicular to the surface. Hence, it cannot strictly describe flows in non-parallel-plate geometries, except in systems targeted in this paper where one has $\nu_s \ll \nu_n$ or ν_s operates only in the inviscid velocity component in the boundary layer. The complete nonlinear HVBK equations (2.1)–(2.4) are then required, rendering the problem analytically intractable. Hence, neglecting vortex tension is the only way an analytic solution can be obtained. Fortunately, in astrophysical applications (e.g. neutron stars), and spin-up in smooth-walled containers, the approximation $\nu_s = 0$ is justified.

2.3. *Interior flow*

For Ekman pumping ($E \ll 1$), it is customary to solve the equations (2.24)–(2.27) for the interior by performing a perturbation expansion in $E^{1/2}$ (Greenspan & Howard 1963; Walin 1969; Abney & Epstein 1996). However, in order to do so, we must specify something about the scale of B and B'. If B is of order unity, then to leading order (2.18) and (2.24) give

$$v_{n\phi} = v_{s\phi} = v_\phi \tag{2.35}$$

and we must proceed to second order in $E^{1/2}$ to solve for the spin-up flow. In this case the inviscid and viscous components are strongly coupled (to leading order in $E^{1/2}$),

https://doi.org/10.1017/jfm.2013.294 Published online by Cambridge University Press

i.e. any differential velocity between the components is removed by mutual friction on the rotational time scale Ω^{-1} and the components are effectively 'locked together' over the Ekman pumping time scale. Alternatively, if B is of order $E^{1/2}$, then terms of order $E^{1/2}$ and smaller can be dropped in (2.24)–(2.27), which then resemble the Greenspan & Howard (1963) equations (5.1) and (5.2) with the addition of the mutual friction coupling terms. With this scaling, differential velocity between the fluid components is removed over the same time scale as Ekman pumping. Therefore the dynamics of the flow depends crucially on the relative size of B and $E^{1/2}$.

A similar effect is seen in stratified flows, where numerical simulations have demonstrated that the relative order of the stratification term appearing in the momentum equation dramatically influences Ekman pumping and the formation of Stewartson layers. Hollerbach (2009) demonstrated that when the stratification parameter S satisfies $S \ll E^{1/2}$, the meridional circulation and temperature scale as $E^{1/2}$ and $E^{-1/2}$, respectively. However, for $S \sim E^{1/2}$, it is found that the meridional circulation speed scales as E, while the temperature becomes independent of E. We might expect similar consequences when adding any other term to the momentum equation, such as the mutual friction. It is therefore informative to solve (2.24)–(2.27) in a way that is valid whether B is smaller than E or vice versa. Then each of the above cases and the transition regimes can be explored as special cases of exact, general formulas. To do this, we neglect all terms of order $E^{1/2}$ and smaller on the left-hand sides of (2.24)–(2.27) (one of which is viscous diffusion), as in previous studies, because they play no role in Ekman pumping. However, we retain the terms on the right-hand sides in which E multiplies the mutual friction coupling constants as these terms may be of any order (not necessarily E) depending on the size of B and B'. Retaining the right-hand terms generalizes previous studies in a way that is practically important, e.g. in astrophysical applications (van Eysden & Melatos 2010). For the interior flow, (2.24)–(2.27) therefore take the form

$$\frac{\partial v_{n\phi}^I}{\partial \tau} + 2\frac{\partial \chi_n^I}{\partial z} = B'\left(\frac{\partial \chi_n^I}{\partial z} - \frac{\partial \chi^I}{\partial z}\right) - BE^{-1/2}\left(v_{n\phi}^I - v_\phi^I\right), \tag{2.36}$$

$$2\frac{\partial v_{n\phi}^I}{\partial z} = B'\left(\frac{\partial v_{n\phi}^I}{\partial z} - \frac{\partial v_\phi^I}{\partial z}\right) + BE^{1/2}\left(\frac{\partial^2 \chi_n^I}{\partial z^2} - \frac{\partial^2 \chi^I}{\partial z^2}\right), \tag{2.37}$$

$$\frac{\partial v_\phi^I}{\partial \tau} + 2\frac{\partial \chi^I}{\partial z} = 0, \tag{2.38}$$

$$2\frac{\partial v_\phi^I}{\partial z} = 0, \tag{2.39}$$

which can be used to solve for the interior flow without specifying the relative size of B and $E^{1/2}$. The special cases $B, B' \sim 1$ and $B, B' \sim E^{1/2}$ can be recovered from the final result, as demonstrated in § 3. Equations (2.36)–(2.39) imply an important generalization of the Taylor–Proudman theorem to the case of two fluids. From (2.38) and (2.39) we find

$$\frac{\partial^2 \chi^I}{\partial z^2} = 0, \tag{2.40}$$

$$\frac{\partial v_\phi^I}{\partial z} = 0, \tag{2.41}$$

https://doi.org/10.1017/jfm.2013.294 Published online by Cambridge University Press

just as in Greenspan & Howard (1963). From (2.36) and (2.37), we find that we must also have

$$\frac{\partial^2 \chi_n^I}{\partial z^2} = 0, \tag{2.42}$$

$$\frac{\partial v_{n\phi}^I}{\partial z} = 0. \tag{2.43}$$

Hence both the inviscid and viscous components must be columnar, i.e. independent of z. Importantly, (2.41) and (2.43) demonstrate that columnarity is preserved for all values of B, unlike in stratified flows, where columnarity is destroyed for $S \gtrsim E^{1/2}$. Columnarity plays an important role in the formation of the Stewartson layers for the case of Couette flow, which is discussed in a companion paper. The solutions for the interior flow can therefore be expressed in the form

$$v_{n\phi}^I = v_{n\phi}^I(r,\tau), \tag{2.44}$$

$$v_{\phi}^I = v_{\phi}^I(r,\tau), \tag{2.45}$$

$$\chi_n^I = -\frac{z}{2}\left[\frac{\partial v_{n\phi}^I}{\partial \tau} + \beta\left(v_{n\phi}^I - v_{\phi}^I\right)\right] + \chi_{0n}^I(r,\tau), \tag{2.46}$$

$$\chi^I = -\frac{z}{2}\frac{\partial v_{\phi}^I}{\partial \tau} + \chi_0^I(r,\tau), \tag{2.47}$$

where we define

$$\beta = \frac{2BE^{-1/2}}{2-B'}. \tag{2.48}$$

This parameter determines the relative importance of the mutual friction parameters, which are explored in more detail in § 3. The unknown quantities $v_{n\phi}^I(r,\tau)$, $v_{\phi}^I(r,\tau)$, $\chi_{0n}^I(r,\tau)$ and $\chi_0^I(r,\tau)$ must be determined from boundary layer physics.

2.4. *Boundary layers*

To solve (2.24)–(2.27) for the boundary layer corrections, we follow Greenspan & Howard (1963) and define the boundary layer variables

$$r = \xi_u + E^{1/2}\zeta_u h_u'(\xi_u) H_u^{-2}(\xi_u), \tag{2.49}$$

$$z = h_u(\xi_u) - E^{1/2}\zeta_u H_u^{-2}(\xi_u) \tag{2.50}$$

for the upper boundary, and

$$r = \xi_l + E^{1/2}\zeta_l h_l'(\xi_l) H_l^{-2}(\xi_l), \tag{2.51}$$

$$z = -h_l(\xi_l) + E^{1/2}\zeta_l H_l^{-2}(\xi_l) \tag{2.52}$$

for the lower boundary, where $\zeta_{u,l}$ is the coordinate normal to the boundaries (scaled by $E^{1/2}$), and $\xi_{u,l}$ is equal to r on the boundaries. We also write

$$H_{u,l}(r) = \left\{1 + \left[\frac{\mathrm{d}h_{u,l}(r)}{\mathrm{d}r}\right]^2\right\}^{1/4}, \tag{2.53}$$

https://doi.org/10.1017/jfm.2013.294 Published online by Cambridge University Press

for brevity. With these transformations, the equations for the upper boundary layer are

$$\frac{\partial^2 v^u_{n\phi}}{\partial \zeta_u^2} + \frac{2}{H_u^2}\frac{\partial \chi^u_n}{\partial \zeta_u} = \frac{B'}{H_u^2}\left(\frac{\partial \chi^u_n}{\partial \zeta_u} - \frac{\partial \chi^u}{\partial \zeta_u}\right) + B\left(v^u_{n\phi} - v^u_\phi\right), \tag{2.54}$$

$$\rho_n \frac{\partial^2 v^u_{n\phi}}{\partial \zeta_u^2} + \frac{2}{H_u^2}\frac{\partial \chi^u}{\partial \zeta_u} = 0, \tag{2.55}$$

$$\frac{\partial^3 \chi^u_n}{\partial \zeta_u^3} - \frac{2}{H_u^2} v^u_{n\phi} = -\frac{B'}{H_u^2}\left(v^u_{n\phi} - v^u_\phi\right) + \frac{B}{H_u^4}\left(\frac{\partial \chi^u_n}{\partial \zeta_u} - \frac{\partial \chi^u}{\partial \zeta_u}\right), \tag{2.56}$$

$$\rho_n \frac{\partial^3 \chi^u_n}{\partial \zeta_u^3} - \frac{2}{H_u^2} v^u_\phi = 0. \tag{2.57}$$

The equations for the lower boundary layer can be obtained from (2.54)–(2.57) by making the replacements $H_u^2 \mapsto -H_l^2$ and $u \mapsto l$ for all subscripts. The no-slip boundary conditions in terms of the boundary layer variables at $\zeta_{u,l} = 0$ are $v^I_{n\phi} + v^{u,l}_{n\phi} = 0$ and $\partial \chi_{u,l}/\partial \zeta_{u,l} = 0$ (since $\partial \chi_I/\partial \zeta_{u,l} = O(E^{1/2})$). Obtaining the solution to (2.54)–(2.57) is mathematically involved, and the reader is referred to the Appendix for details. The results for the upper boundary layer corrections to the streamfunctions are

$$\chi^u_n = \tfrac{1}{2}\left(rf_u - v^I_{n\phi}\right)\left(I_{u-}\cos\lambda_{u+}\zeta_u + I_{u+}\sin\lambda_{u+}\zeta_u\right)\mathrm{e}^{-\lambda_{u-}\zeta_u}, \tag{2.58}$$

$$\chi^u = \tfrac{1}{2}\left(rf_u - v^I_{n\phi}\right)\left(J_{u-}\cos\lambda_{u+}\zeta_u + J_{u+}\sin\lambda_{u+}\zeta_u\right)\mathrm{e}^{-\lambda_{u-}\zeta_u}, \tag{2.59}$$

and for the lower boundary layer

$$\chi^l_n = -\tfrac{1}{2}\left(rf_l - v^I_{n\phi}\right)\left(I_{l-}\cos\lambda_{l+}\zeta_l + I_{l+}\sin\lambda_{l+}\zeta_l\right)\mathrm{e}^{-\lambda_{l-}\zeta_l}, \tag{2.60}$$

$$\chi^l = -\tfrac{1}{2}\left(rf_l - v^I_{n\phi}\right)\left(J_{l-}\cos\lambda_{l+}\zeta_l + J_{l+}\sin\lambda_{l+}\zeta_l\right)\mathrm{e}^{-\lambda_{l-}\zeta_l}, \tag{2.61}$$

in terms of the functions

$$I_{u,l\pm} = \frac{1}{|\lambda_{u,l}|^2\lambda_{u,l\pm}}\left[\left(\frac{1-H_{u,l}^4}{1+H_{u,l}^4}\right)^2\left(\lambda_{u,l+}^2 - \lambda_{u,l-}^2\right)^2 + 4\lambda_{u,l+}^2\lambda_{u,l-}^2\right]^{1/2}, \tag{2.62}$$

$$J_{u,l\pm} = \frac{\rho_n H_{u,l}^2}{2\lambda_{u,l\pm}\left(1+H_{u,l}^4\right)}\left[|\lambda_{u,l}|^2\left(1-H_{u,l}^4\right) + 4\lambda_{u,l\pm}^2 H_{u,l}^4\right], \tag{2.63}$$

with

$$\lambda_{u,l\pm} = \frac{1}{H_{u,l}}\left\{\left[\frac{(B'-2)^2 + B^2}{(\rho_n B'-2)^2 + (\rho_n B)^2}\right]^{1/2} \mp \frac{\rho_s B\left(1+H_{u,l}^4\right)}{H_{u,l}^2\left[(\rho_n B'-2)^2 + (\rho_n B)^2\right]}\right\}^{1/2}, \tag{2.64}$$

$$|\lambda_{u,l}|^2 = \lambda_{u,l-}^2 + \lambda_{u,l+}^2. \tag{2.65}$$

For the velocities, we find

$$v^{u,l}_{n\phi} = \left(rf_{u,l} - v^I_{n\phi}\right)\left(\cos\lambda_{u,l+}\zeta_{u,l} + C_{u,l+}\sin\lambda_{u,l+}\zeta_{u,l}\right)\mathrm{e}^{-\lambda_{u,l-}\zeta_{u,l}}, \tag{2.66}$$

$$C_{u,l+} = \frac{\left(1-H_{u,l}^4\right)\left(\lambda_{u,l-}^2 - \lambda_{u,l+}^2\right)}{2\lambda_{u,l+}\lambda_{u,l-}\left(1+H_{u,l}^4\right)}, \tag{2.67}$$

$$v^{u,l}_\phi = \left(rf_{u,l} - v^I_{n\phi}\right)\left(D_{u,l-}\cos\lambda_{u,l+}\zeta_{u,l} + D_{u,l+}\sin\lambda_{u,l+}\zeta_{u,l}\right)\mathrm{e}^{-\lambda_{u,l-}\zeta_{u,l}}, \tag{2.68}$$

https://doi.org/10.1017/jfm.2013.294 Published online by Cambridge University Press

$$D_{u,l-} = \frac{\rho_n H_{u,l}^2}{2}\left[\left(\frac{1-H_{u,l}^4}{1+H_{u,l}^4}\right)^2\left(\lambda_{u,l+}^2-\lambda_{u,l-}^2\right)^2+4\lambda_{u,l+}^2\lambda_{u,l-}^2\right]^{1/2}, \tag{2.69}$$

$$D_{u,l+} = \frac{\rho_n H_{u,l}^2\left(\lambda_{u,l+}^2-\lambda_{u,l-}^2\right)}{4\lambda_{u,l+}\lambda_{u,l-}}\left[\left(\frac{1-H_{u,l}^4}{1+H_{u,l}^4}\right)^2\left(\lambda_{u,l+}^2-\lambda_{u,l-}^2\right)^2+4\lambda_{u,l+}^2\lambda_{u,l-}^2\right]^{1/2}. \tag{2.70}$$

From (2.58)–(2.61), we see that the boundary layer thickness scales as $LE^{1/2}\lambda_{u,l-}^{-1}$. Therefore $\lambda_{u,l-}$ adjusts the boundary layer thickness according to the shape of the boundary and the coupling of the two fluid components. This modifies the flow structure according to the functions $J_{u,l\pm}$, $I_{u,l\pm}$, $C_{u,l+}$, $D_{u,l\pm}$. As with the interior, the flow in the boundary layer depends strongly on the size of B and B'. We discuss this further in § 3.

2.5. *No-penetration boundary conditions and temporal evolution*

The temporal evolution of the interior flow is determined by applying the no-penetration boundary condition (Greenspan & Howard 1963). This is done for the viscous component and the total fluid on the upper and lower boundaries. At $z = h_u$ we require

$$\chi_n^I + \chi_n^u = 0, \tag{2.71}$$

$$\chi^I + \chi^u = 0. \tag{2.72}$$

Similarly, at $z = -h_l$, we require

$$\chi_n^I + \chi_n^l = 0, \tag{2.73}$$

$$\chi^I + \chi^l = 0. \tag{2.74}$$

Substituting the expressions (2.46), (2.47), (2.58)–(2.61) into (2.71)–(2.74), we obtain

$$h_u\left[\frac{\partial v_{n\phi}^I}{\partial\tau}+\beta\left(v_{n\phi}^I-v_\phi^I\right)\right]-2\chi_{0n}^I = I_{u-}\left(rf_u-v_{n\phi}^I\right), \tag{2.75}$$

$$h_u\frac{\partial v_\phi^I}{\partial\tau}-2\chi_0^I = J_{u-}\left(rf_u-v_{n\phi}^I\right), \tag{2.76}$$

$$h_l\left[\frac{\partial v_{n\phi}^I}{\partial\tau}+\beta\left(v_{n\phi}^I-v_\phi^I\right)\right]+2\chi_{0n}^I = I_{l-}\left(rf_l-v_{n\phi}^I\right), \tag{2.77}$$

$$h_l\frac{\partial v_\phi^I}{\partial\tau}+2\chi_0^I = J_{l-}\left(rf_l-v_{n\phi}^I\right), \tag{2.78}$$

which gives four ordinary differential equations in the unknown quantities $v_{n\phi}^I(r,\tau)$, $v_\phi^I(r,\tau)$, $\chi_{0n}^I(r,\tau)$ and $\chi_0^I(r,\tau)$, where τ plays the role of the independent variable. Upon eliminating χ_{0n}^I and χ_0^I, the system reduces to two coupled, first-order, ordinary differential equations:

$$\frac{\partial v_\phi^I}{\partial\tau}+\frac{J_{u-}+J_{l-}}{h_u+h_l}v_{n\phi}^I = r\frac{J_{u-}f_u+J_{l-}f_l}{h_u+h_l}, \tag{2.79}$$

$$\frac{\partial v_{n\phi}^I}{\partial\tau}+\left[\beta+\frac{I_{u-}+I_{l-}}{h_u+h_l}\right]v_{n\phi}^I-\beta v_\phi^I = \frac{r\left(I_{u-}f_u+I_{l-}f_l\right)}{h_u+h_l}. \tag{2.80}$$

https://doi.org/10.1017/jfm.2013.294 Published online by Cambridge University Press

Eliminating $v^I_{n\phi}(r,\tau)$ we obtain

$$\frac{\partial^2 v^I_\phi}{\partial\tau^2}+\left(\beta+\frac{I_{u-}+I_{l-}}{h_u+h_l}\right)\frac{\partial v^I_\phi}{\partial\tau}+\beta\left(\frac{J_{u-}+J_{l-}}{h_u+h_l}\right)v^I_\phi = \frac{r}{h_u+h_l}\left[J_{u-}\left(\frac{\partial f_u}{\partial\tau}+\beta f_u\right)+J_{l-}\left(\frac{\partial f_l}{\partial\tau}+\beta f_l\right)\right]. \tag{2.81}$$

In (2.81) only v^I_ϕ and $f_{u,l}$ depend on τ. Therefore, when the right-hand side is zero, the left-hand side reduces to a second-order, homogeneous ordinary differential equation with constant coefficients (which depend only on r and not τ). Its solutions are of the form $\exp(\omega_\pm\tau)$, with

$$\omega_\pm=-\frac{1}{2}\left(\beta+\frac{I_{u-}+I_{l-}}{h_u+h_l}\right)\pm\left\{\left[\frac{1}{2}\left(\beta+\frac{I_{u-}+I_{l-}}{h_u+h_l}\right)\right]^2-\beta\left(\frac{J_{u-}+J_{l-}}{h_u+h_l}\right)\right\}^{1/2}. \tag{2.82}$$

The particular solutions can be obtained by the method of variation of parameters (Zwillinger 1989), which utilizes the Wronskian of the complementary homogeneous solutions. Applying the initial conditions $v^I_{n\phi}(r,0)=r\Omega_{n0}$, $v^I_\phi(r,0)=r\Omega_0$ at $\tau=0$, the solution is

$$\begin{aligned} v^I_\phi = \frac{r}{\omega_+-\omega_-}\Bigg\{&\int_0^\tau \mathrm{d}\tau'\left[\frac{J_{u-}f_u(\tau')+J_{l-}f_l(\tau')}{h_u+h_l}\right]\left[(\omega_++\beta)\,\mathrm{e}^{\omega_+(\tau-\tau')}\right.\\ &\left.-(\omega_-+\beta)\,\mathrm{e}^{\omega_-(\tau-\tau')}\right]-\Omega_0\left(\omega_-\mathrm{e}^{\omega_+\tau}-\omega_+\mathrm{e}^{\omega_-\tau}\right)\\ &-\Omega_{n0}\left(\frac{J_{u-}+J_{l-}}{h_u+h_l}\right)\left(\mathrm{e}^{\omega_+\tau}-\mathrm{e}^{\omega_-\tau}\right)\Bigg\}, \end{aligned} \tag{2.83}$$

$$\begin{aligned} v^I_{n\phi} = \frac{r}{\omega_+-\omega_-}\Bigg\{&\int_0^\tau \mathrm{d}\tau'\left[\frac{J_{u-}f_u(\tau')+J_{l-}f_l(\tau')}{J_{u-}+J_{l-}}\right][\omega_-(\omega_-+\beta)\mathrm{e}^{\omega_-(\tau-\tau')}\\ &-\omega_+(\omega_++\beta)\,\mathrm{e}^{\omega_+(\tau-\tau')}]+\beta\Omega_0\left(\mathrm{e}^{\omega_+\tau}-\mathrm{e}^{\omega_-\tau}\right)\\ &+\Omega_{n0}(\omega_+\mathrm{e}^{\omega_+\tau}-\omega_-\mathrm{e}^{\omega_-\tau})\Bigg\}. \end{aligned} \tag{2.84}$$

For completeness, we also quote the solutions for the interior stream functions obtained from (2.46), (2.47) and (2.75)–(2.78), that is,

$$\chi^I_n=\frac{I_{u-}\left(v^I_{n\phi}-rf_u\right)(z+h_l)+I_{l-}\left(v^I_{n\phi}-rf_l\right)(z-h_u)}{2\,(h_u+h_l)}, \tag{2.85}$$

$$\chi^I=\frac{J_{u-}\left(v^I_{n\phi}-rf_u\right)(z+h_l)+J_{l-}\left(v^I_{n\phi}-rf_l\right)(z-h_u)}{2\,(h_u+h_l)}. \tag{2.86}$$

The results (2.85)–(2.86) are useful for obtaining the torque on the container, which is considered in § 5.

The spin-up of a symmetric container to a constant angular velocity is typically studied classically (Greenspan & Howard 1963; Pedlosky 1967; Walin 1969; Abney &

https://doi.org/10.1017/jfm.2013.294 Published online by Cambridge University Press

Epstein 1996). Taking $f_u(\tau) = f_l(\tau) = 1$ and $h_u(r) = h_l(r)$, (2.83) and (2.84) become

$$v_\phi^I = r + \left(\frac{rJ_-}{h}\right)\left(\frac{1-\Omega_{n0}}{\omega_+ - \omega_-}\right)(\mathrm{e}^{\omega_+\tau} - \mathrm{e}^{\omega_-\tau}) + r\left(\frac{1-\Omega_0}{\omega_+ - \omega_-}\right)(\omega_-\mathrm{e}^{\omega_+\tau} - \omega_+\mathrm{e}^{\omega_-\tau}), \tag{2.87}$$

$$v_{n\phi}^I = r - r\left(\frac{1-\Omega_{n0}}{\omega_+ - \omega_-}\right)(\omega_+\mathrm{e}^{\omega_+\tau} - \omega_-\mathrm{e}^{\omega_-\tau}) - r\beta\left(\frac{1-\Omega_0}{\omega_+ - \omega_-}\right)(\mathrm{e}^{\omega_+\tau} - \mathrm{e}^{\omega_-\tau}) \tag{2.88}$$

where we drop the u, l subscripts. In the classical limit, $B = B' = 0$ and $\rho_n = 1$, we obtain $\beta = \omega_+ = 0$, $\omega_- = -H/h$, and $\Omega_0 = \Omega_{n0}$, and the solution of Greenspan & Howard (1963) for the spin-up of a single-component, viscous fluid in a container of arbitrary shape is recovered.

3. Mutual friction

The analytic solution in § 2 enjoys many practical applications, which are explored in companion papers (van Eysden & Melatos 2010, 2011, 2012). In this section, we investigate instead how the spin-up process is influenced by mutual friction. According to the discussion in § 2.3, the new physics depends on the relative size of the parameter β, defined in (2.48). In a neutron star, we expect $B \ll$ and $B' \sim B^2$ (Mendell 1991*b*; van Eysden & Melatos 2010) so that B' is negligible. In this case, β can be regarded as the ratio of the Ekman time to the time scale for the dissipative component of the mutual friction to bring the two fluid components into co-rotation. In helium II, the mutual friction coefficients remain relatively constant over the temperature range $1.30\ \mathrm{K} < T < 2.10\ \mathrm{K}$, with $1.298 < B < 1.526$ and $-0.065 < B' < 0.616$. The mutual coefficients diverge as the superfluid transition temperature is approached, with $B = 12.693$, $B' = -8.172$ at $T = 2.1767$ K. The cases of strong ($\beta \gg 1$), intermediate ($\beta \sim 1$) and weak ($\beta \ll 1$) coupling limits are investigated separately.

3.1. *Strong coupling*

Let us first consider the regime $\beta \gg 1$. Figure 1 presents the spin-up flow in a sphere (with $h_u(r) = h_l(r) = \left(1 - r^2\right)^{1/2}$), which is spun up to a constant angular velocity with $f_u(\tau) = f_l(\tau) = 1$ (see (2.87) and (2.88)). Slices of the meridional flow for the viscous (figure 1*a,c,e*) and inviscid (figure 1*b,d,f*) components are plotted at three different times, $\tau = 0.2$ (*a,b*), 1 (*c,d*), and 5 (*e,f*). Both fluid components participate in Ekman pumping; the attendant circulation follows the contours, which represent poloidal streamlines. The viscous component undergoes classical Ekman pumping, while the inviscid component is dragged along, because it is strongly coupled by mutual friction. The magnitude of the angular velocity is also displayed in colour. It evolves from zero everywhere (in the rotating frame) at $\tau = 0$ to $v_\phi^I/r = v_{n\phi}^I/r = 1$ as $\tau \to \infty$. Both components spin up in concert, as seen from the identical shading in panels (*a,c,e*) and (*b,d,f*). Again, this is because the two fluid components are locked together in the strong-coupling limit by mutual friction, with $v_\phi^I = v_{n\phi}^I$, as discussed in § 2.3.

The qualitative features in the previous paragraph make sense analytically. Expanding $\omega_\pm$ in (2.82) in powers of $E^{1/2} \ll 1$, we find

$$\omega_+ = -J_-/h, \tag{3.1}$$

$$\omega_- = -\beta. \tag{3.2}$$

https://doi.org/10.1017/jfm.2013.294 Published online by Cambridge University Press

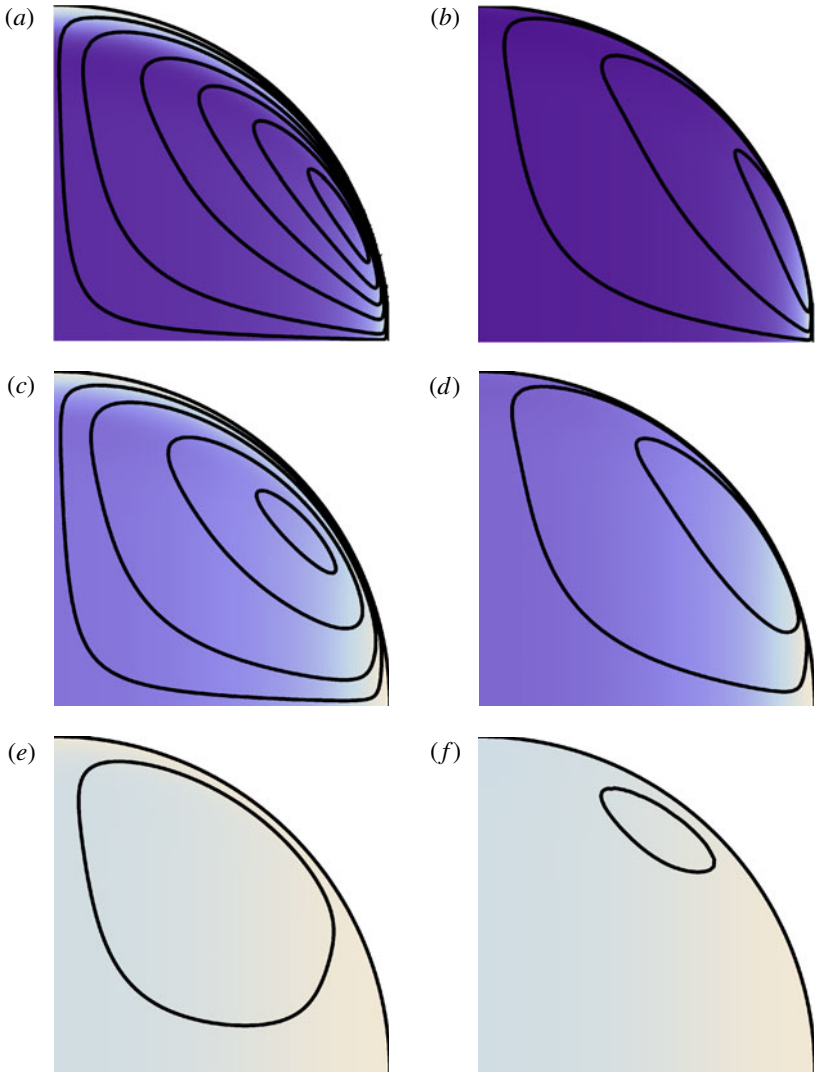


FIGURE 1. (Colour online) Slices of the meridional flow for the viscous (*a,c,e*) and inviscid (*b,d,f*) components for strong coupling. Snapshots are for (*a,b*) $\tau = 0.2$, (*c,d*) $\tau = 1$ and (*e,f*) $\tau = 5$. The superfluid parameters are $B = 1$, $B' = 0$, $E = 0.005$, $\rho_n = 0.25$. The initial conditions are $\Omega_{n0} = \Omega_0 = 0$ in the rotating frame. Poloidal flow is clockwise with contours (from bottom left): -0.005, -0.025, -0.075, -0.125, -0.175, -0.225. The magnitude of the angular velocity (in the rotating frame) is displayed in colour, where dark is zero and light is unity (spun up).

to leading order. Here, β is $O(E^{-1/2})$; hence we have $|\omega_-| \gg |\omega_+|$. Equations (2.87) and (2.88) then reduce to

$$v^I_\phi = r\,[1 - (1 - \Omega_0)\,\mathrm{e}^{\omega_+\tau}]\,, \tag{3.3}$$

$$v^I_{n\phi} = r\,[1 - (\Omega_0 - \Omega_{n0})\,\mathrm{e}^{\omega_-\tau} - (1 - \Omega_0)\,\mathrm{e}^{\omega_+\tau}]\,. \tag{3.4}$$

https://doi.org/10.1017/jfm.2013.294 Published online by Cambridge University Press

Equation (3.3) has the classical form, with spin-up time $h/(J_- E^{1/2}\Omega)$, where the function J_- encodes the strong coupling between the two fluids. The viscous component (3.4) contains an extra term which, from the definition (2.48), decays on the time scale $(2 - B')/(2B\Omega)$. For $\beta \gg 1$, this time scale resembles the rotation period, which is much faster than the Ekman pumping time scale. In other words, differential rotation between the viscous and inviscid components is removed quickly, as anticipated in § 2.3. An advantage of solving for the interior flow using (2.36)–(2.39) is that this rapid decay of any differential rotation appears explicitly in the solution. This term would not appear if we assume $B \sim O(1)$ before solving (2.36)–(2.39) using a perturbation expansion in $E^{1/2}$.

To explore the role of B', we re-plot the panels in figure 1, choosing $B = 5$ and $B' = -8$ so that β is unchanged. These values are similar to those in helium II near the superfluid transition temperature, where experiments are frequently conducted. We find that the streamlines are slightly sparser in figure 2, indicating that the velocity of the secondary flow is weaker than in figure 1 at a given time. However, the qualitative features remain the same and spin-up still occurs on the Ekman time for both viscous and inviscid components components. Because B' does not play a dominant role in the spin-up dynamics, we do not explore its effect in the intermediate and weak coupling regimes below.

3.2. *Intermediate coupling*

In figure 3 we present results from the intermediate coupling regime, $\beta \sim 1$. The panels represent snapshots at the same times as in figure 1. From panels (*a,c,e*), we see that the viscous component undergoes classic Ekman pumping, and its streamlines correspond closely to the strong-coupling regime (figure 1*a,c,e*). In contrast, panels (*b,d,f*) now have no contours, indicating that the poloidal flow for the inviscid component is very slow. The mutual friction force is now too weak to drag along the inviscid component on the Ekman time scale, unlike in figure 1. The different shadings in panels (*a,c,e*) and (*b,d,f*) indicate that the $O(1)$ azimuthal velocities for the inviscid and viscous components spin up at different rates. The spin-up rates mix together the Ekman time scale and the mutual friction time scale. To appreciate this, consider the analytical solution. For $B, B' \ll 1$ (implied by $E^{1/2} \ll 1$), (2.62)–(2.64) reduce to

$$\lambda_{u,l\pm} = H_{u,l}^{-1}, \tag{3.5}$$

$$J_{u,l-} = J_{u,l+} = \rho_n H_{u,l}, \tag{3.6}$$

$$I_{u,l-} = I_{u,l+} = H_{u,l}, \tag{3.7}$$

$$C_{u,l+} = D_{u,l+} = 0, \tag{3.8}$$

$$D_{u,l-} = \rho_n. \tag{3.9}$$

We find $\chi = \rho_n \chi_n$ and hence $\chi_s = 0$, reflecting the dearth of contours in figure 3(*b,d,f*). Moreover, because we have $\beta \sim O(1)$, both ω_+ and ω_- are the same order of magnitude, and (2.82) does not simplify significantly. Therefore, the spin-up time for the viscous and inviscid components in this limit is a complex mixture of the mutual friction and Ekman time scales.

3.3. *Weak coupling*

Finally, let us consider the weak coupling regime, $\beta \ll 1$. As the behaviour is qualitatively similar to intermediate coupling, we do not present flow streamlines.

https://doi.org/10.1017/jfm.2013.294 Published online by Cambridge University Press

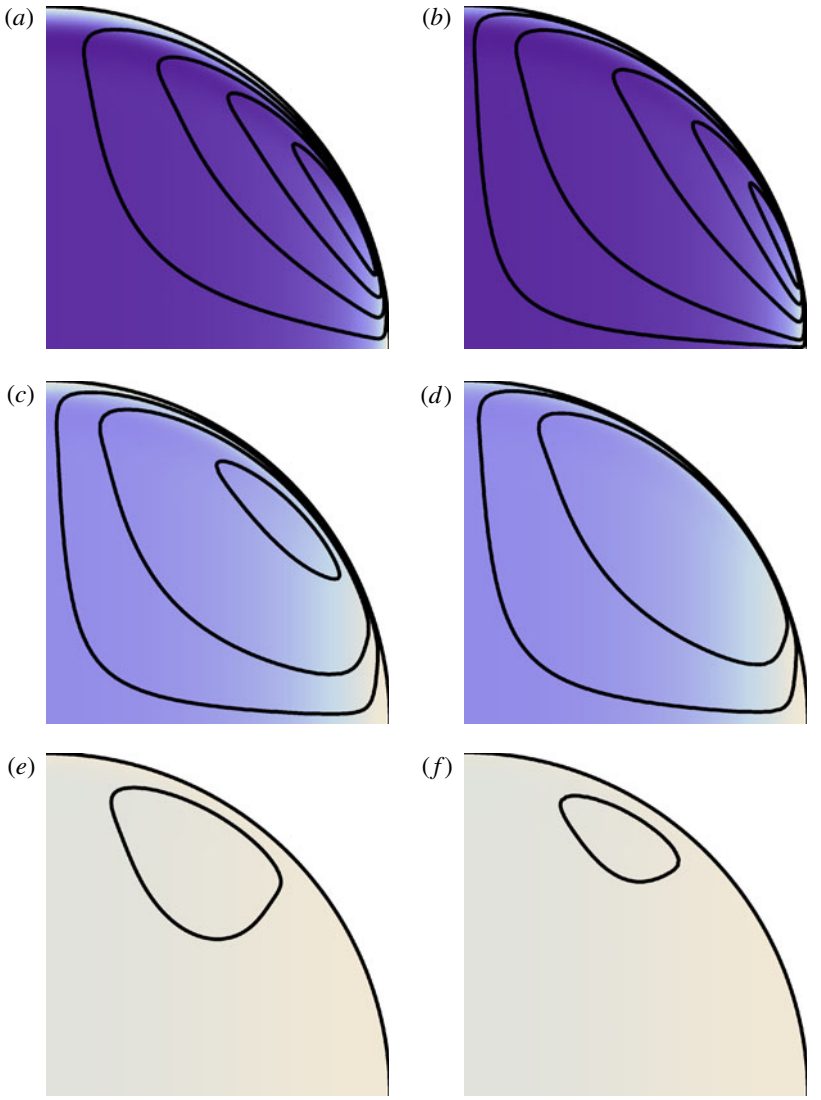


FIGURE 2. (Colour online) Slices of the meridional flow for the viscous (*a,c,e*) and inviscid (*b,d,f*) components for $B = 5$, $B' = -8$, $E = 0.005$. All other details identical to figure 1.

Equations (3.5)–(3.9) apply, so the inviscid component does not circulate poloidally, just as for intermediate coupling. For $\beta \sim O(E^{1/2})$, the exponents are

$$\omega_+ = -\rho_n \beta, \tag{3.10}$$

$$\omega_- = -H/h \tag{3.11}$$

to leading order. With $|\omega_-| \gg |\omega_+|$, (2.87) and (2.88) become

$$v^I_\phi = r\left[1 - \rho_n\left(1 - \Omega_{n0}\right)\mathrm{e}^{\omega_- \tau} - \rho_s\left(1 - \Omega_{s0}\right)\mathrm{e}^{\omega_+ \tau}\right], \tag{3.12}$$

$$v^I_{n\phi} = r\left[1 - \left(1 - \Omega_{n0}\right)\mathrm{e}^{\omega_- \tau}\right]. \tag{3.13}$$

https://doi.org/10.1017/jfm.2013.294 Published online by Cambridge University Press

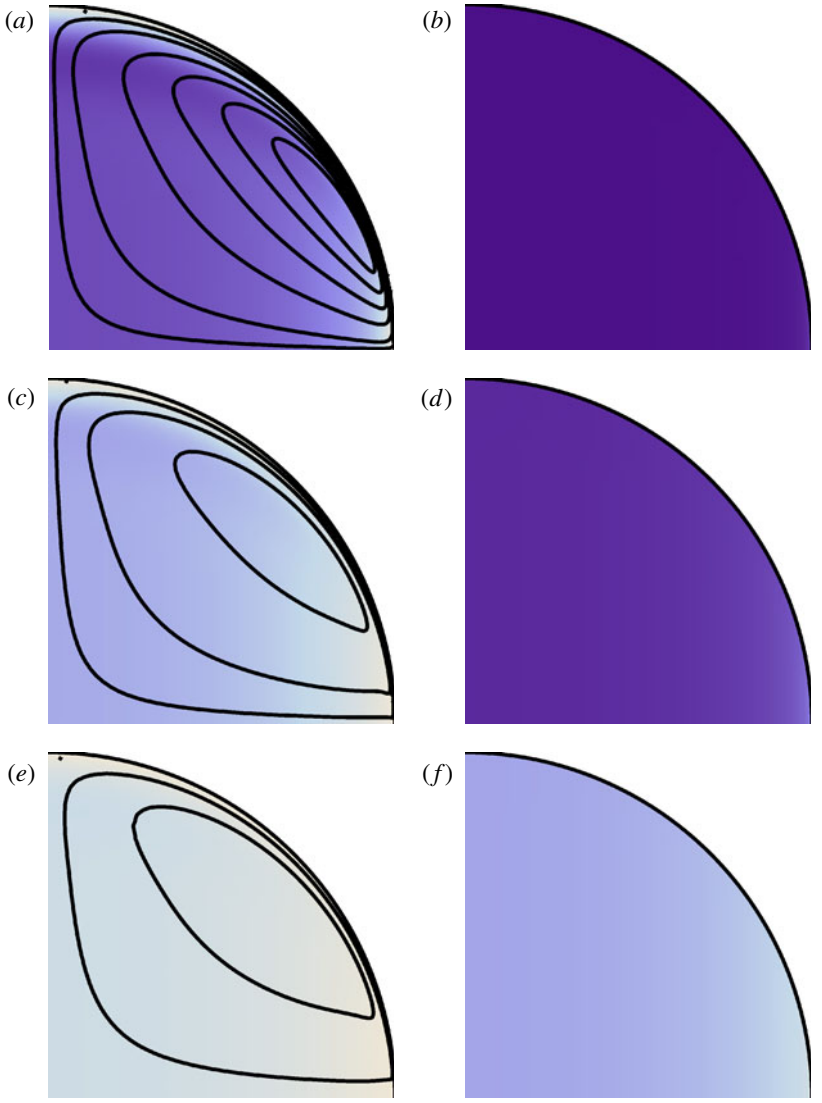


FIGURE 3. (Colour online) Slices of the meridional flow for the viscous (*a,c,e*) and inviscid (*b,d,f*) components for intermediate coupling ($B = 0.071$, $B' = 0$, $E = 0.005$). All other details identical to figure 1.

Equation (3.13) describes the classic spin-up for a viscous fluid uninhibited by the inviscid component, with spin-up time $h/(HE^{1/2}\Omega)$. The inviscid component spins up via mutual friction over the much longer time scale $(B\rho_n\Omega)^{-1}$.

In each of the above regimes, the parameter β in (2.48) determines the strength of the coupling rather than B or B' individually. For example, if B is of order $O(1)$, then β is $O(E^{-1/2})$ if B' is $O(1)$ or $O(E^{1/2})$. Similarly, for $B \lesssim E^{1/2}$, one finds $\beta \approx BE^{-1/2}$, irrespective of the scale of B' (note that $B' \leqslant 2$). Therefore, the spin-up of two fluids coupled by a mutual friction force of the Hall–Vinen form (2.6) depends most strongly on the relative size of B and $E^{1/2}$. This is not surprising, because B and $E^{1/2}$ control the time scales for the two dissipative processes in the flow. $E^{-1/2}\Omega^{-1}$ is the time scale

https://doi.org/10.1017/jfm.2013.294 Published online by Cambridge University Press

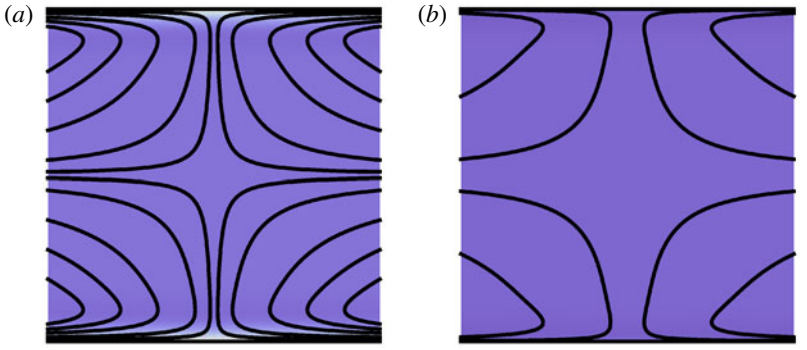


FIGURE 4. (Colour online) Slices of the meridional flow for the viscous (*a*) and inviscid (*b*) components in a cylinder for strong coupling, with all model parameters identical to figure 1. Snapshots are for $\tau = 1$. Poloidal flow is clockwise in the top-right corner and the contours have the same values as for figure 1 (from the centre outwards). The flow is mirrored about the vertical and horizontal bisectors in the other quadrants.

for viscous dissipation when Ekman pumping is occurring. The B term in the mutual friction force (2.6) corresponds to a dissipative drag force, which arises from inelastic scattering between the viscous component and the vortex cores, and brings the two fluid components into co-rotation on the time scale $(B\Omega)^{-1}$. In contrast, the B' term is not dissipative. It arises from the Bernoulli force exerted on a vortex when there is differential rotation between the fluid components.

4. Container geometry

In this section, we apply the solution in § 2 to explore the new physics arising from different container shapes and rotational symmetries. We pay special attention to two geometries, a cylinder and a cone, which are relevant to many of the laboratory and astrophysical applications to be analysed in future work.

4.1. *Cylinder*

The spin-up of a two-component superfluid in a sphere is explored in § 3. By way of comparison, we now present the corresponding solution in cylindrical geometry, where $h_u(r) = h_l(r) = 1$. The half-height and radius of the cylinder are equal to the radius of the sphere studied in § 3. In figure 4, we plot a snapshot of the poloidal streamlines and toroidal flow speed at $\tau = 1$, after the container spins up to a constant angular velocity with $f_u(\tau) = f_l(\tau) = 1$. All model parameters are identical to those in figure 1, and the snapshot corresponds to panels (*c,d*) in the latter figure. In contrast with figure 1, we plot all four quadrants of the container. The flow is clockwise in the top-right corner and mirrored about the vertical and horizontal bisectors in the other quadrants.

According to the two-fluid extension of the Taylor–Proudman theorem, discussed in § 2.3, the leading-order Ekman flow is columnar. This is evident in both the sphere and cylinder in figures 1–4; the shading is striped vertically in all panels. The evolution of a column of fluid between r and $r + \mathrm{d}r$ is determined by the boundary conditions at its top and bottom, $z = \pm h(r)$, the inclination angle of the boundaries, parametrized by $H(r)$, and the superfluid parameters B, B', ρ_n and E. Comparing figure 1(*c,d*) and figure 4, the fluid spins up faster in a sphere at larger radii, where the fluid columns are shorter, and the inclination angle is steeper.

https://doi.org/10.1017/jfm.2013.294 Published online by Cambridge University Press

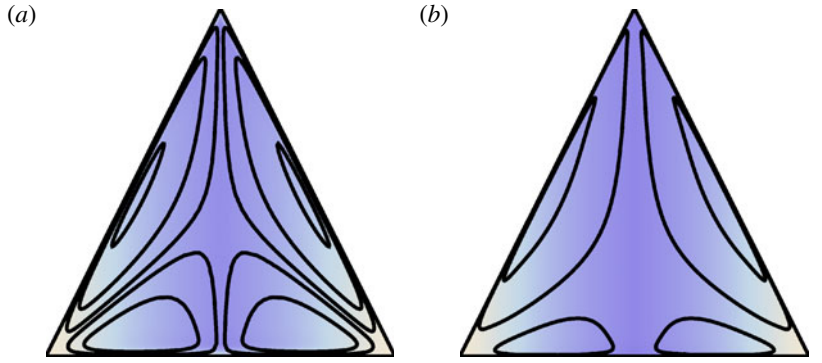


FIGURE 5. (Colour online) Slices of the meridional flow for the viscous (*a*) and inviscid (*b*) components in a cone for strong coupling, with all model parameters identical to figure 1. Snapshots are for $\tau = 1$. Flow is clockwise adjacent to the right wall, anti-clockwise adjacent to the lower right boundary, and mirrored about the rotation axis. Contours: from centre to top right, -0.005, -0.025, -0.075; from centre to bottom right, 0.005, 0.025.

We note in passing that there is an important interplay between columnarity and boundary conditions at the vertical sidewalls of the container. The no-penetration and no-slip boundary conditions at the vertical boundary are satisfied by two nested vertical boundary layers of thickness $E^{1/4}$ and $E^{1/3}$, known as the Stewartson layers. These layers also transport any $O(E^{1/2})$ mass flux from the top and bottom Ekman layers back into the interior, completing the Ekman pumping cycle (Greenspan & Howard 1963). The Stewartson layers only form on vertical boundaries; they are not present in a sphere, where the Ekman layer performs the above functions. Solving for these layers is involved, and irrelevant to the interior flow, so we do not study them here. For more details the reader is referred to Greenspan (1968).

4.2. *Cone*

As another illustrative example, consider a cone with $h_u(r) = 1 - (\cot\theta)\, r$, where 2θ is the opening angle, and $h_l(r) = 1$.

In figure 5 we plot a snapshot of the flow in a cone with $\theta = 26.6^\circ$ at $\tau = 1$, after the container has been impulsively accelerated to a constant angular velocity $f_u(\tau) = f_l(\tau) = 1$. All other model parameters are identical to figure 1. To facilitate comparison, the height of the cone is equal to the total height of the sphere and cylinder considered in figures 1–4.

As in the previous examples, a clockwise poloidal circulation is induced adjacent to the upper-right boundary (sidewall of the cone) and an anti-clockwise poloidal circulation is induced adjacent to the base of the cone, mirrored about the rotation axis. The flow is qualitatively similar to that in a cylinder and a sphere, but adjusted to fit the shape of the cone. At large r, the azimuthal velocity spins up more than in the cylinder or sphere by $\tau = 1$, because the fluid columns are shorter. For larger opening angles θ (keeping the height constant), figure 5 stretches horizontally, with the contour values and colour scale remaining the same.

4.3. *Counter-rotating top and bottom*

As another illustrative example of the utility and generality of the solution in § 2, we consider a cylinder whose top and bottom are not rigidly connected and are

https://doi.org/10.1017/jfm.2013.294 Published online by Cambridge University Press

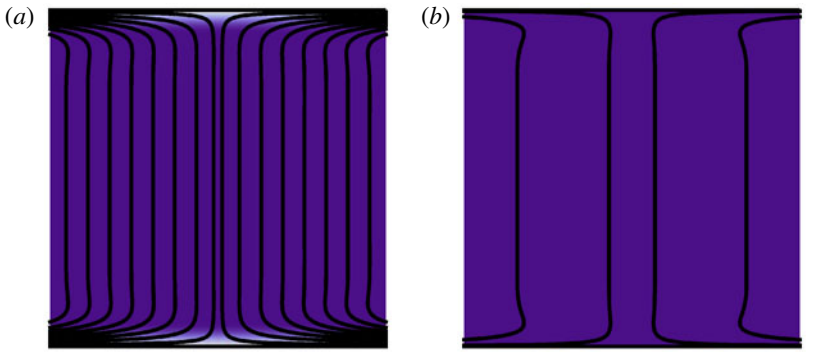


FIGURE 6. (Colour online) Slices of the meridional flow for the viscous (*a*) and inviscid (*b*) in a cylinder with counter-rotating top and bottom. The fluid components are strongly coupled, with all superfluid parameters identical to figure 1. Poloidal flow is clockwise on the right-hand side of the rotation axis, with contours (from the centre outwards): -0.01, -0.05, -0.10, -0.15, -0.20, -0.25. The flow is mirrored about the rotation axis on the left-hand side.

impulsively accelerated in opposite directions ($f_u = -f_l = 1$). The resulting flow is plotted in figure 6 for $\Omega_{n0} = \Omega_0 = 0$. As in previous figures, the poloidal circulation of the inviscid component (figure 6*b*) is weaker than the circulation in the viscous component (figure 6*a*), even though the coupling is strong ($B = 1$). Interestingly, the anti-symmetry in the boundary conditions guarantees that there is no transient flow for these initial conditions. After the boundary layer forms, the flow immediately assumes a steady-state solution, with $v^I_\phi = v^I_{n\phi} = 0$, as seen in figure 6 (uniform shading). However, the differential rotation of the boundaries drives a persistent poloidal flow, which follows the contours in figure 6. In the upper boundary layer, the Coriolis force drives an $O(E^{1/2})$ flow radially outwards, just as in previous figures. In the lower boundary layer, the counter-motion of the wall results in an $O(E^{1/2})$ flow which points radially inwards. To satisfy continuity requirements, the inflow in the lower boundary layer is directed into the interior, where it is drawn into the upper boundary and pumped back outwards. In a similar manner to figure 4, the cycle is completed by Stewartson layers on the vertical sidewalls, which transport the $O(E^{1/2})$ outflow in the upper boundary layer to the lower boundary layer. The same qualitative behaviour is observed in other counter-rotating geometries with $f_u = -f_l = 1$. In a sphere and a cone, the Ekman layer transports the $O(E^{1/2})$ flow from the upper boundary to the lower boundary, from where it is pumped back through the interior to complete the cycle.

The flows in figures 4 and 6 can be used to explore all possibilities for the spin-up of upper and lower surfaces to constant angular velocities; any other flow can be constructed as a linear superposition of these two examples. For example, given $f_u = 1$ and $f_l = 0$, the solution can be constructed by adding the flows in figures 4 and 6 (and dividing by two). Immediately after the spin-up, in this example, a radial outflow develops in the upper boundary layer, but there is no flow in the lower boundary layer. As $t \to \infty$, a persistent poloidal flow develops as a result of the boundary shear, just as in figure 6. The azimuthal velocity approaches rigid body rotation (similar to figure 4), with angular velocity equal to the average of the upper and lower boundary.

In some geometries, the sense of rotation of the boundaries can impact the stability of the Stewartson layers. In spherical Couette geometry, counter-rotating boundaries

https://doi.org/10.1017/jfm.2013.294 Published online by Cambridge University Press

become more unstable than co-rotating boundaries, as Ω is increased (Hollerbach 2003).

4.4. *Parallel plates*

Finally, we compare our general results with the strong-coupling solution for parallel plates accelerating at a slow ($\dot{f} \ll f$) and constant rate. This system was studied by Reisenegger (1993) and is the only detailed spin-up solution for an HVBK superfluid published to date. We now demonstrate exact agreement in that limit.

In parallel-plate geometry, we have $h = H = 1$, and (2.62)–(2.64) reduce to

$$I_{u-} = I_{l-} = \frac{2\lambda_+}{|\lambda|^2}, \tag{4.1}$$

$$J_{u-} = J_{l-} = \rho_n \lambda_- , \tag{4.2}$$

$$\lambda_\pm = \left\{ \left[\frac{(B'-2)^2 + B^2}{(\rho_n B' - 2)^2 + (\rho_n B)^2} \right]^{1/2} \mp \frac{2\rho_s B}{(\rho_n B' - 2)^2 + (\rho_n B)^2} \right\}^{1/2}. \tag{4.3}$$

Reisenegger (1993) treated the regime where the inviscid and viscous components are strongly coupled, i.e. $B, B' \sim O(1)$. Hence the result (3.1) applies: the spin-up time t_s, defined as reciprocal of ω_+, takes the form

$$t_s = \left(\rho_n \lambda_- E^{1/2} \Omega\right)^{-1}. \tag{4.4}$$

The transport coefficients B, B' in the HVBK theory are related to the coefficients β_0, β_0' introduced by Chandler & Baym (1986) according to

$$B = \frac{2\rho}{\rho_n} \frac{\beta_0}{\left(1 + \beta_0'\right)^2 + \beta_0^2}, \tag{4.5}$$

$$B' = \frac{2\rho}{\rho_n} \frac{\beta_0' + \beta_0'^2 + \beta_0^2}{\left(1 + \beta_0'\right)^2 + \beta_0^2}. \tag{4.6}$$

After some algebraic manipulation, (4.4)–(4.6) combine to give

$$t_s = \left(\rho_n E^{1/2} \Omega\right)^{-1} \left\{ \left[\left(1 - \frac{\beta_0' \rho_s}{\rho_n}\right)^2 + \left(\frac{\beta_0 \rho_s}{\rho_n}\right)^2 \right]^{1/2} + \frac{\beta_0 \rho_s}{\rho_n} \right\}^{-1/2}, \tag{4.7}$$

which is identical to (58) in Reisenegger (1993).

5. Torque on the container

In this section, we derive an expression for the hydrodynamic torque T exerted on the container by the viscous component of the superfluid. This result is useful in its own right; we show below that the torque is an excellent diagnostic of the Ekman process for different coupling strengths and container shapes when plotted as a function of time. It is also an essential piece of the self-consistent coupled spin-up of a superfluid and its vessel, to be analysed in a forthcoming paper.

First, we consider the upper half of the container. The infinitesimal torque element $\mathrm{d}T_u$ between r and $r + \mathrm{d}r$ is given by

$$\mathrm{d}T_u = r[\boldsymbol{e}_\phi \cdot \boldsymbol{T} \cdot \boldsymbol{n}_u]_{z=h_u} \mathrm{d}A, \tag{5.1}$$

https://doi.org/10.1017/jfm.2013.294 Published online by Cambridge University Press

where $\boldsymbol{T}$ is the viscous stress tensor, scaled to $\rho L^2 \epsilon \Omega^2$. Equation (5.1) is evaluated at the boundary, $z = h_u$. The surface area element and the unit normal at the upper boundary are respectively

$$\mathrm{d}A = 2\pi r H_u^2 \mathrm{d}r, \tag{5.2}$$

$$\boldsymbol{n}_u = H_u^{-2} \left(\frac{\mathrm{d}h}{\mathrm{d}r} \boldsymbol{e}_r - \boldsymbol{e}_z \right). \tag{5.3}$$

Writing the stress tensor in component form, and using the relations (A 1) and (A 2), we obtain

$$\boldsymbol{e}_\phi \cdot \boldsymbol{T} \cdot \boldsymbol{n}_u = \rho_n E^{1/2} \frac{\partial v_{n\phi}}{\partial \zeta_u}, \tag{5.4}$$

To leading order, we have $\partial v_{n\phi}/\partial \zeta_u \approx \partial v^u_{n\phi}/\partial \zeta_u$, as $\partial v^I_{n\phi}/\partial \zeta_u \sim O(E^{1/2})$. From the boundary layer equation (A 8), and the boundary conditions for χ (2.71), we find

$$\left[\frac{\partial v^u_{n\phi}}{\partial \zeta_u} \right]_{\zeta_u = 0} = \frac{2}{\rho_n H_u^2} \left[\chi^I \right]_{z = h_u}. \tag{5.5}$$

Substituting (5.2) and (5.5) into (5.1) and integrating, we obtain

$$T_u = 4\pi E^{1/2} \int_0^R \mathrm{d}r\, r^2 \left[\chi^I \right]_{z = h_u} \tag{5.6}$$

for the total torque on the upper lid, where R denotes the dimensionless maximum cylindrical radius of the vessel. Following a similar procedure at the lower boundary layer, we obtain

$$T_l = -4\pi E^{1/2} \int_0^R \mathrm{d}r\, r^2 \left[\chi^I \right]_{z = -h_l}. \tag{5.7}$$

Using (2.79) and (2.86), the torque can be written in terms of the total azimuthal velocity as

$$T_u = -2\pi E^{1/2} \int_0^R \mathrm{d}r \left(\frac{J_{u-} r^2}{J_{u-} + J_{l-}} \right) \left[(h_u + h_l) \frac{\partial v^I_\phi}{\partial \tau} + r J_{l-} (f_u - f_l) \right], \tag{5.8}$$

$$T_l = -2\pi E^{1/2} \int_0^R \mathrm{d}r \left(\frac{J_{l-} r^2}{J_{u-} + J_{l-}} \right) \left[(h_u + h_l) \frac{\partial v^I_\phi}{\partial \tau} - r J_{u-} (f_u - f_l) \right]. \tag{5.9}$$

In figure 7, we plot the torque (calculated from (5.8) and (5.9)) versus time for the flows presented in previous figures. The short-dashed and long-dashed curves correspond to the flows in a sphere presented in figures 1 and 3 respectively. The solid and dot-dashed curves correspond to the torques on the cylinder (presented in figure 4) and the cone (presented in figure 5) respectively. Because of the differential rotation in figure 6, the torque on the upper lid is constant, with $T_u E^{-1/2} = -0.239$ (the torque on the lower lid is equal but opposite), and is not included in figure 7.

In a sphere, the torque on the container is not an exponential function of time. This is because the spin-up time of a column of fluid between r and $r + \mathrm{d}r$ changes with r, as discussed in § 4.1. Therefore, the total torque on the container is a weighted sum of the torques at different r, each with a different characteristic time scale. Compared with the cylinder, the torque on the sphere is greater initially and diminishes more rapidly, because the fluid at large r spins up more quickly. The short-dashed curve

https://doi.org/10.1017/jfm.2013.294 Published online by Cambridge University Press

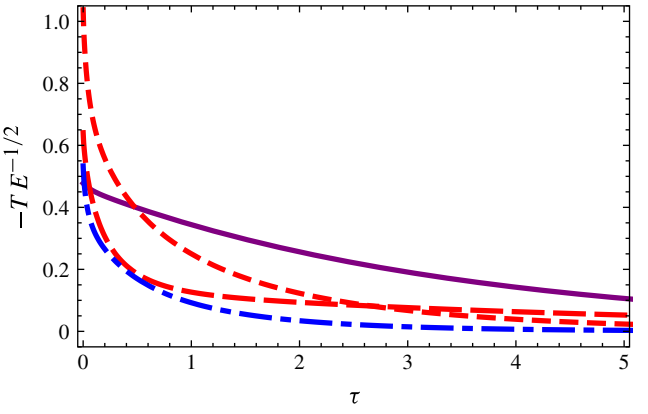


FIGURE 7. (Colour online) Torque exerted on the container by the fluid versus time for the spin-up flows considered in figures 1–5. The red short-dashed and red long-dashed curves correspond to the strong- and intermediate-coupling flows in a sphere presented in figures 1 and 3 respectively. The purple solid and blue dot-dashed curves correspond to the cylinder (figure 4) and the cone (figure 5) respectively.

has a larger initial torque than the long-dashed curve, because the fluid components are strongly coupled. The areas under both dashed curves are identical, because the amount of fluid spun up and therefore the angular impulse imparted to the fluid are the same in both cases. Similarly, the torque on the cone is a non-exponential function of time. The area under the curve is smaller than for a sphere, reflecting the smaller volume of fluid.

In contrast to the sphere and cone, the spin-up time of a fluid column in a cylinder is not a function of r. The torque is the sum of two exponentials, which can easily be calculated analytically from (2.87) and (5.8)–(5.9). The cylinder has the largest area under its curve, because it has the largest volume.

Besides their relevance to figure 7, the formulas in this section will serve as an important reference for future papers, where we calculate the coupled spin-down of the superfluid and its container self-consistently in both simply connected and spherical Couette geometries, and compare the results to laboratory and astrophysical measurements.

6. Comparison with experiments

The theory presented in this paper has been tested against the results of spin-up experiments performed by the Tsakadze group over a decade (Tsakadze & Tsakadze 1972, 1973, 1974, 1980), as discussed in § 2.2. To connect the theory with the observed response of the container, an additional calculation, which is performed in a companion paper, is needed for the self-consistent motion of the container under the combined action of internal (due to viscosity) and external (due to friction in the apparatus) torques.

The detailed experimental comparison is published in van Eysden & Melatos (2011). Here we summarize the key findings for the benefit of the reader. In the experiments, the angular velocity of a helium-II-filled sphere measuring 3.4 cm in diameter is impulsively increased from 3.0 to 4.2 rad s^{-1}. The subsequent relaxation of the container is measured until the container decelerates linearly. The spin-up

https://doi.org/10.1017/jfm.2013.294 Published online by Cambridge University Press

time is defined as the moment at which the motion of the container transitions from exponential to linear deceleration. This experiment is repeated at six temperatures in the range $1.46\ \mathrm{K} < T < 2.22\ \mathrm{K}$.

Excellent agreement (error $\approx 0.5\,\%$) is achieved at $T = 1.57\ \mathrm{K}$ when comparing directly the experimental spin-down curve in smooth-walled containers with that predicted by the theory presented in this paper using the generally accepted thermodynamic properties of helium II compiled by Donnelly (2012) (see figure 2 of van Eysden & Melatos 2011). The predicted spin-up times in the temperature range $1.46\ \mathrm{K} < T < 1.8\ \mathrm{K}$ were also found to be consistent with observations (see figure 4 of van Eysden & Melatos (2011)). Poorer agreement is found under conditions where turbulence is excited, e.g. higher angular velocity (5.0 to 6.5 rad s^{-1}), and rough-walled containers.

The results of van Eysden & Melatos (2011) suggest that there is a range of experimental conditions for helium II under which the linear theory neglecting vortex tension presented in this paper is valid. As discussed in § 2.2, the requirement for laminar Ekman pumping $\epsilon < E^{1/2} < 1$ is satisfied where experimental agreement is found, while turbulence is expected for $T > 1.6\ \mathrm{K}$. For the experiments performed in more rapidly rotating containers (5.0 rad s^{-1}), turbulence is expected at all temperatures where experimental data are available.

7. Conclusions

An analytic solution to the HVBK equations has been presented which solves for the spin-up of both the viscous and inviscid components of a superfluid in arbitrary geometry. The solution generalizes previous studies of single-component Navier–Stokes fluids in arbitrary geometry and two-component HVBK spin-up between parallel plates.

Unlike stratified flows, where the columnarity is destroyed when the stratification is strong, a two-component fluid coupled by Hall–Vinen mutual friction preserves columnarity for all values of B. The spin-up time for a fluid column between r and $r + \mathrm{d}r$ is a function of its height and the inclination angle of its upper and lower boundaries. In a sphere and a cone, the fluid at large r spins up faster where the container shortens, while in a cylinder the spin-up time is independent of r. Columnarity controls the formation of Stewartson layers on the sidewalls, which is important in the simple geometries considered here, as well as non-simply connected geometries (such as spherical Couette) which will be analysed in a future paper.

By considering the strong ($\beta \gg 1$), intermediate ($\beta \sim 1$) and weak ($\beta \ll 1$) coupling regimes, we demonstrate that the spin-up of a two-component superfluid depends crucially on the relative scale of B and $E^{1/2}$. For $\beta \gg 1$, the inviscid component undergoes Ekman pumping because it is dragged along by the viscous component, and the azimuthal velocities are locked together over the Ekman time scale. For $\beta \lesssim 1$, there is no poloidal flow in the inviscid component, while the azimuthal inviscid component spins up by mutual friction over a combination of the Ekman and mutual friction time scales. The solution captures the physics for any choice of the mutual friction coupling constants B and B'.

The temporal evolution of the torque exerted on the container following the impulsive acceleration is a combination of the spin-up times of fluid columns at different r. The torque formulas (5.2) and (5.5) will be a key input in a forthcoming paper on the coupled spin-up problem, where the container responds self-consistently to the back-reaction torque of the viscous component of the superfluid, and the

https://doi.org/10.1017/jfm.2013.294 Published online by Cambridge University Press

boundary conditions on the superfluid are likewise continually and self-consistently adjusted.

The analytic solutions derived in this paper are applicable to glitch recovery in neutron stars (van Eysden & Melatos 2010), and spin-down experiments involving helium II and other terrestrial superfluids in smooth-walled containers (van Eysden & Melatos 2011, 2012), where the vortex tension is much less than the kinematic viscosity or is confined to the inviscid velocity component in the boundary layer and exerts a marginal influence on the spin-up dynamics globally.

Acknowledgement

C.A.V.E. acknowledges the financial support of an Australian Postgraduate Award.

Appendix. Boundary layers

A.1. *Upper boundary layer*

A.1.1. *Equations*

With the transformations (2.49) and (2.50), the gradient operators in the upper boundary layer transform as

$$\frac{\partial}{\partial r} = E^{-1/2}\frac{h_u'(\xi_u)}{H_u^2}\frac{\partial}{\partial \zeta_u}, \tag{A 1}$$

$$\frac{\partial}{\partial z} = -E^{-1/2}\frac{1}{H_u^2}\frac{\partial}{\partial \zeta_u}, \tag{A 2}$$

$$\mathscr{L} = E^{-1}\frac{\partial^2}{\partial \zeta^2}. \tag{A 3}$$

Using these definitions, (2.24)–(2.27) in the upper boundary layer reduce to

$$\frac{\partial^2 v_{n\phi}^u}{\partial \zeta_u^2} + \frac{2}{H_u^2}\frac{\partial \chi_n^u}{\partial \zeta_u} = \frac{B'}{H_u^2}\left(\frac{\partial \chi_n^u}{\partial \zeta_u} - \frac{\partial \chi^u}{\partial \zeta_u}\right) + B\left(v_{n\phi}^u - v_\phi^u\right), \tag{A 4}$$

$$\rho_n\frac{\partial^2 v_{n\phi}^u}{\partial \zeta_u^2} + \frac{2}{H_u^2}\frac{\partial \chi^u}{\partial \zeta_u} = 0, \tag{A 5}$$

$$\frac{\partial^3 \chi_n^u}{\partial \zeta_u^3} - \frac{2}{H_u^2}v_{n\phi}^u = -\frac{B'}{H_u^2}\left(v_{n\phi}^u - v_\phi^u\right) + \frac{B}{H_u^4}\left(\frac{\partial \chi_n^u}{\partial \zeta_u} - \frac{\partial \chi^u}{\partial \zeta_u}\right), \tag{A 6}$$

$$\rho_n\frac{\partial^3 \chi_n^u}{\partial \zeta_u^3} - \frac{2}{H_u^2}v_\phi^u = 0. \tag{A 7}$$

Solving these equations, from (A 5) and (A 7) we obtain

$$\chi^u = -\frac{\rho_n H_u^2}{2}\frac{\partial v_{n\phi}^u}{\partial \zeta_u}, \tag{A 8}$$

$$v_\phi^u = \frac{\rho_n H_u^2}{2}\frac{\partial^3 \chi_n^u}{\partial \zeta_u^3}. \tag{A 9}$$

https://doi.org/10.1017/jfm.2013.294 Published online by Cambridge University Press

Substituting (A 8) and (A 9) into (A 4) and (A 6) and rearranging, we arrive at a quartic system of ordinary differential equations,

$$\left(ac-b^2\right)^{1/2}\frac{\partial\chi_n^u}{\partial\zeta_u}=-H_u^2\left(a\frac{\partial^2 v_{n\phi}^u}{\partial\zeta_u^2}+bv_{n\phi}^u\right), \tag{A 10}$$

$$H_u^2\left(ac-b^2\right)^{1/2}\frac{\partial^3\chi_n^u}{\partial\zeta_u^3}=\left(b\frac{\partial^2 v_{n\phi}^u}{\partial\zeta_u^2}+cv_{n\phi}^u\right), \tag{A 11}$$

with

$$a=\left(\rho_n B'-2\right)^2+(\rho_n B)^2, \tag{A 12a}$$

$$b=-4\rho_s B, \tag{A 12b}$$

$$c=4\left[\left(B'-2\right)^2+B^2\right], \tag{A 12c}$$

$$\left(ac-b^2\right)^{1/2}=2\left\{\rho_n\left[\left(B'-2\right)^2+B^2\right]-2\rho_s\left(B'-2\right)\right\}. \tag{A 12d}$$

Combining (A 10) and (A 11), we find

$$\left[aH_u^4\frac{\partial^4}{\partial\zeta_u^4}+b\left(1+H_u^4\right)\frac{\partial^2}{\partial\zeta_u^2}+c\right]v_{n\phi}^u=0. \tag{A 13}$$

Equation (A 13) governs the boundary layer corrections. Assuming linear solutions of the form $\mathrm{e}^{\lambda\zeta_u}$, (A 13) becomes

$$aH_u^4\lambda^4+b\left(1+H_u^4\right)\lambda^2+c=0. \tag{A 14}$$

The solutions to (A 14) are

$$\lambda=\pm\lambda_-\pm\mathrm{i}\lambda_+, \tag{A 15}$$

$$\lambda_{u\pm}=\left[\left(\frac{c}{4aH_u^4}\right)^{1/2}\pm\frac{b\left(1+H_u^4\right)}{4aH_u^4}\right]^{1/2}. \tag{A 16}$$

The boundary layer corrections must decay to be transcendentally small away from the boundary, so we keep only the exponentially decaying solutions of (A 16). To determine these, note that c, a and H_u are always positive, so that $c/(4aH_u^4)$ is always real. When the discriminant $b^2\left(1+H_u^4\right)^2-4acH_u^4$ is negative, then λ_- and λ_+ are both always real, and correspond to the real and imaginary components of the solution respectively. When the discriminant is positive, and b is negative (as is the case here), then λ_+ becomes purely imaginary; but $|\lambda_+|<|\lambda_-|$ implies that λ is always real and negative. Therefore, if we consider the solution

$$\lambda_u=-\lambda_{u-}+\mathrm{i}\lambda_{u+}, \tag{A 17}$$

its real component is negative definite (the same holds for its complex conjugate λ_u^*). These are the solutions required. Writing in terms of the superfluid coefficients, we have

$$\lambda_{u\pm}=\frac{1}{H_u}\left\{\left[\frac{(B'-2)^2+B^2}{(\rho_n B'-2)^2+(\rho_n B)^2}\right]^{1/2}\mp\frac{\rho_s B\left(1+H_u^4\right)}{H_u^2\left[(\rho_n B'-2)^2+(\rho_n B)^2\right]}\right\}^{1/2}, \tag{A 18}$$

https://doi.org/10.1017/jfm.2013.294 Published online by Cambridge University Press

which reduces to H_u^{-1} in the limit $B, B' \to 0$, $\rho_n \to 1$ as required (Greenspan & Howard 1963).

The general solution for the boundary layer velocity is

$$v^u_{n\phi} = \tfrac{1}{2}\left(\xi_u f_u - v^I_{n\phi}\right)\left(C^*_u \mathrm{e}^{\lambda_u \zeta_u} + C_u \mathrm{e}^{\lambda^*_u \zeta_u}\right), \tag{A 19}$$

where we anticipate the real pre-factor $(\xi_u f_u - v^I_{n\phi})/2$ based on the form of Greenspan's result. Using (A 10), we find

$$\chi^u_n = \tfrac{1}{4}\left(\xi_u f_u - v^I_{n\phi}\right)\left(I^*_u \mathrm{e}^{\lambda_u \zeta_u} + I_u \mathrm{e}^{\lambda^*_u \zeta_u}\right), \tag{A 20}$$

where we define the complex coefficient

$$I_u = -\frac{2H_u^2\left(a\lambda_u^{*2} + b\right) C_u}{\lambda^*_u\left(ac - b^2\right)^{1/2}}. \tag{A 21}$$

Similarly, using (A 8) and (A 9), we write

$$\chi^u = \tfrac{1}{4}(\xi_u f_u - v^I_{n\phi})(J^*_u \mathrm{e}^{\lambda_u \zeta_u} + J_u \mathrm{e}^{\lambda^*_u \zeta_u}), \tag{A 22}$$

$$v^u_\phi = \tfrac{1}{2}(\xi_u f_u - v^I_{n\phi})(D^*_u \mathrm{e}^{\lambda_u \zeta_u} + D_u \mathrm{e}^{\lambda^*_u \zeta_u}), \tag{A 23}$$

and we define the complex coefficients

$$J_u = -\rho_n H_u^2 \lambda^*_u C_u, \tag{A 24}$$

$$D_u = \tfrac{1}{4}\rho_n H_u^2 \lambda^{*3}_u I_u. \tag{A 25}$$

A.1.2. *No-slip boundary conditions*

To determine the constant C_u in (A 21) and (A 24) we need to consider the no-slip boundary conditions at $z = h_u(\xi)$, which require

$$v^I_{n\phi} + v^u_{n\phi} = \xi_u f_u, \tag{A 26}$$

$$\frac{\partial \chi^u_n}{\partial \zeta_u} = 0. \tag{A 27}$$

Using (A 19) and (A 20), we have

$$C^*_u + C_u = 2, \tag{A 28}$$

$$\lambda_u I^*_u + \lambda^*_u I_u = 0. \tag{A 29}$$

Solving with (A 21), we obtain

$$C_u = \frac{2\left(a\lambda_u^2 + b\right)}{a\left(\lambda_u^2 - \lambda_u^{*2}\right)}, \tag{A 30}$$

$$I_u = -\frac{4\left(ac - b^2\right)^{1/2}}{aH_u^2\lambda^*_u\left(\lambda_u^2 - \lambda_u^{*2}\right)}. \tag{A 31}$$

Making use of the relations

$$\frac{b}{a} = -\frac{H_u^4\left(\lambda_u^2 + \lambda_u^{*2}\right)}{1 + H_u^4}, \tag{A 32a}$$

$$\frac{c}{a} = \left(\lambda_u \lambda^*_u\right)^2 H_u^4, \tag{A 32b}$$

https://doi.org/10.1017/jfm.2013.294 Published online by Cambridge University Press

we find

$$C_u = 1 + \left(\frac{1-H_u^4}{1+H_u^4}\right)\left(\frac{\lambda_u^2+\lambda_u^{*2}}{\lambda_u^2-\lambda_u^{*2}}\right), \tag{A 33}$$

$$I_u = \frac{2}{\lambda_u^*\left(\lambda_u^{*2}-\lambda_u^2\right)}\left[\left(\frac{1-H_u^4}{1+H_u^4}\right)^2\left(\lambda_u^2+\lambda_u^{*2}\right)^2 - \left(\lambda_u^{*2}-\lambda_u^2\right)^2\right]^{1/2}. \tag{A 34}$$

Note that the term in the square brackets is always positive. Since $\left(\lambda_u^{*2}-\lambda_u^2\right)$ is complex, it is safest to leave the pre-factor outside the square brackets to avoid errors when taking the square root. Writing out all complex numbers in terms of their real and imaginary components, we obtain the results (2.62)–(2.63) for the upper boundary layer where the '−' and '+' subscripts denote the real and imaginary components respectively when the discriminant is positive.

A.2. *Lower boundary layer*

A.2.1. *Equations*

The gradient operators transform as

$$\frac{\partial}{\partial r} = E^{-1/2}\frac{h_i'(\xi_u)}{H_l^2}\frac{\partial}{\partial \zeta_l}, \tag{A 35}$$

$$\frac{\partial}{\partial z} = E^{-1/2}\frac{1}{H_l^2}\frac{\partial}{\partial \zeta_l}. \tag{A 36}$$

Using these definitions, (2.24)–(2.27) in the lower boundary layer reduce to

$$\frac{\partial^2 v_{n\phi}^l}{\partial \zeta_l^2} - \frac{2}{H_l^2}\frac{\partial \chi_n^l}{\partial \zeta_l} = -\frac{B'}{H_l^2}\left(\frac{\partial \chi_n^l}{\partial \zeta_l} - \frac{\partial \chi^l}{\partial \zeta_l}\right) + B\left(v_{n\phi}^l - v_\phi^l\right), \tag{A 37}$$

$$\rho_n\frac{\partial^2 v_{n\phi}^l}{\partial \zeta_l^2} - \frac{2}{H_l^2}\frac{\partial \chi^l}{\partial \zeta_l} = 0, \tag{A 38}$$

$$\frac{\partial^3 \chi_n^l}{\partial \zeta_l^3} + \frac{2}{H_l^2}v_{n\phi}^l = \frac{B'}{H_l^2}\left(v_{n\phi}^l - v_\phi^l\right) + \frac{B}{H_l^4}\left(\frac{\partial \chi_n^l}{\partial \zeta_l} - \frac{\partial \chi^l}{\partial \zeta_l}\right), \tag{A 39}$$

$$\rho_n\frac{\partial^3 \chi_n^l}{\partial \zeta_l^3} + \frac{2}{H_l^2}v_\phi^l = 0. \tag{A 40}$$

Inspecting (A 37)–(A 40), we note that the lower boundary layer equations can be obtained from the upper boundary layer (2.54)–(2.57) by making the substitution $H_u^2 \mapsto -H_l^2$. The azimuthal flow fields and poloidal stream functions are then given by

$$v_{n\phi}^l = \tfrac{1}{2}(\xi_l f_l - v_{n\phi}^I)(C_l^* \mathrm{e}^{\lambda_l \zeta_l} + C_l \mathrm{e}^{\lambda_l^* \zeta_l}), \tag{A 41}$$

$$v_\phi^l = \tfrac{1}{2}(\xi_l f_l - v_{n\phi}^I)(D_l^* \mathrm{e}^{\lambda_l \zeta_l} + D_l \mathrm{e}^{\lambda_l^* \zeta_l}), \tag{A 42}$$

$$\chi_n^l = -\tfrac{1}{4}(\xi_l f_l - v_{n\phi}^I)(I_l^* \mathrm{e}^{\lambda_l \zeta_l} + I_l \mathrm{e}^{\lambda_l^* \zeta_l}), \tag{A 43}$$

$$\chi^l = -\tfrac{1}{4}(\xi_l f_l - v_{n\phi}^I)(J_l^* \mathrm{e}^{\lambda_l \zeta_l} + J_l \mathrm{e}^{\lambda_l^* \zeta_l}), \tag{A 44}$$

where we define the complex coefficients

$$C_l = 1 + \left(\frac{1-H_l^4}{1+H_l^4}\right)\left(\frac{\lambda_l^2+\lambda_l^{*2}}{\lambda_l^2-\lambda_l^{*2}}\right), \tag{A 45}$$

https://doi.org/10.1017/jfm.2013.294 Published online by Cambridge University Press

$$I_l = \frac{2}{\lambda_l^* \left(\lambda_l^{*2} - \lambda_l^2\right)} \left[\left(\frac{1 - H_l^4}{1 + H_l^4} \right)^2 \left(\lambda_l^2 + \lambda_l^{*2}\right)^2 - \left(\lambda_l^{*2} - \lambda_l^2\right)^2 \right]^{1/2}, \tag{A 46}$$

$$J_l = -\rho_n H_l^2 \lambda_l^* C_l, \tag{A 47}$$

$$D_l = \frac{1}{4} \rho_n H_l^2 \lambda_l^{*3} I_l. \tag{A 48}$$

REFERENCES

ABNEY, M. & EPSTEIN, R. I. 1996 Ekman pumping in compact astrophysical bodies. *J. Fluid Mech.* **312**, 327–340.

ADAMS, P. W., CIEPLAK, M. & GLABERSON, W. I. 1985 Spin-up problem in superfluid ^{4}He. *Phys. Rev.* B **32**, 171–177.

AMBERG, G. & UNGARISH, M. 1993 Spin-up from rest of a mixture: numerical simulation and asymptotic theory. *J. Fluid Mech.* **246**, 443–464.

ANDERSON, P. W. & ITOH, N. 1975 Pulsar glitches and restlessness as a hard superfluidity phenomenon. *Nature* **256**, 25–27.

ANDERSON, P. W., PINES, D., RUDERMAN, M. & SHAHAM, J. 1978 Questions about rotating superfluid dynamics: problems of pulsar astrophysics accessible in the laboratory. *J. Low Temp. Phys.* **30**, 839–847.

ANDERSSON, N., SIDERY, T. & COMER, G. L. 2006 Mutual friction in superfluid neutron stars. *Mon. Not. R. Astron. Soc.* **368**, 162–170.

BARENGHI, C. F. 1992 Vortices and the Couette flow of helium II. *Phys. Rev.* B **45**, 2290–2293.

BARENGHI, C. F., DONNELLY, R. J. & VINEN, W. F. 1983 Friction on quantized vortices in helium II. A review. *J. Low Temp. Phys.* **52**, 189–247.

BARENGHI, C. F. & JONES, C. A. 1988 The stability of the Couette flow of helium II. *J. Fluid Mech.* **197**, 551–569.

BAYM, G. & CHANDLER, E. 1983 The hydrodynamics of rotating superfluids. Part 1. Zero-temperature, nondissipative theory. *J. Low Temp. Phys.* **50**, 57–87.

BAYM, G., EPSTEIN, R. I. & LINK, B. 1992 Dynamics of vortices in neutron stars. *Phys.* B *Condens. Matter* **178**, 1–12.

BAYM, G., PETHICK, C. & PINES, D. 1969 Superfluidity in neutron stars. *Nature* **224**, 673–674.

BENTON, E. R. & CLARK, A. 1974 Spin-up. *Annu. Rev. Fluid Mech.* **6**, 257–280.

BENTON, E. R. & LOPER, D. E. 1969 On the spin-up of an electrically conducting fluid. Part 1. The unsteady hydromagnetic Ekman–Hartmann boundary-layer problem. *J. Fluid Mech.* **39**, 561–586.

BONDI, H. & LYTTLETON, R. A. 1948 On the dynamical theory of the rotation of the earth. *Proc. Camb. Phil. Soc.* **44**, 345–359.

CAMPBELL, L. J. & KRASNOV, Y. K. 1982 Transient behavior of rotating superfluid helium. *J. Low Temp. Phys.* **49**, 377–396.

CHANDLER, E. & BAYM, G. 1986 The hydrodynamics of rotating superfluids. Part 2. Finite temperature, dissipative theory. *J. Low Temp. Phys.* **62**, 119–142.

CUTLER, C. & LINDBLOM, L. 1987 The effect of viscosity on neutron star oscillations. *Astrophys. J.* **314**, 234–241.

DONNELLY, R. J. 2005 *Quantized Vortices in Helium II*. Cambridge University Press.

DONNELLY, R. J. 2012 URL: http://darkwing.uoregon.edu/~rjd/vapor1.htm.

DREW, D. A. & PASSMAN, S. L. 1999 *Theory of Multicomponent Fluids*. Springer.

EASSON, I. 1979 Postglitch behavior of the plasma inside neutron stars. *Astrophys. J.* **228**, 257–267.

ELTSOV, V. B., DE GRAAF, R., HEIKKINEN, P. J., HOSIO, J. J., HÄNNINEN, R., KRUSIUS, M. & L'VOV, V. S. 2010 Stability and dissipation of laminar vortex flow in superfluid ^{3}He-B. *Phys. Rev. Lett.* **105** (12), 125301.

https://doi.org/10.1017/jfm.2013.294 Published online by Cambridge University Press

FINNE, A. P., ARAKI, T., BLAAUWGEERS, R., ELTSOV, V. B., KOPNIN, N. B., KRUSIUS, M., SKRBEK, L., TSUBOTA, M. & VOLOVIK, G. E. 2003 An intrinsic velocity-independent criterion for superfluid turbulence. *Nature* **424**, 1022–1025.

GEURST, J. A. 1988 Drift mass, multifluid modelling of two-phase bubbly flow and superfluid hydrodynamics. *Phys.* A *Stat. Mech. Appl.* **152**, 1–28.

GLABERSON, W. I., JOHNSON, W. W. & OSTERMEIER, R. M. 1974 Instability of a vortex array in He II. *Phys. Rev. Lett.* **33**, 1197–1200.

GLAMPEDAKIS, K., ANDERSSON, N. & SAMUELSSON, L. 2011 Magnetohydrodynamics of superfluid and superconducting neutron star cores. *Mon. Not. R. Astron. Soc.* **410**, 805–829.

GRAVITATIONAL WAVE INTERNATIONAL COMMITTEE, 2012 URL: https://gwic.ligo.org/.

GREENSPAN, H. P. 1968 *The Theory of Rotating Fluids*. Cambridge Monographs on Mechanics and Applied Mathematics, Cambridge University Press, xii+328 pp.

GREENSPAN, H. P. & HOWARD, L. N. 1963 On a time-dependent motion of a rotating fluid. *J. Fluid Mech.* **17**, 385–404.

HENDERSON, K. L. & BARENGHI, C. F. 2000 The anomalous motion of superfluid helium in a rotating cavity. *J. Fluid Mech.* **406**, 199–219.

HENDERSON, K. L. & BARENGHI, C. F. 2004 Superfluid Couette flow in an enclosed annulus. *Theor. Comput. Fluid Dyn.* **18**, 183–196.

HENDERSON, K. L., BARENGHI, C. F. & JONES, C. A. 1995 Nonlinear Taylor–Couette flow of helium II. *J. Fluid Mech.* **283**, 329–340.

HILLS, R. N. & ROBERTS, P. H. 1977 Superfluid mechanics for a high density of vortex lines. *Arch. Rat. Mech. Anal.* **66**, 43–71.

HOLLERBACH, R. 2003 Instabilities of the Stewartson layer. Part 1. The dependence on the sign of *Ro*. *J. Fluid Mech.* **492**, 289–302.

HOLLERBACH, R. 2009 Instabilities of Taylor columns in a rotating stratified fluid. *Phys. Lett.* A **373**, 3775–3778.

ISHII, M. & MISHIMA, K. 1984 Two fluid model and hydrodynamic constitutive relations. *Nucl. Engng Des.* **82**, 107–126.

KHALATNIKOV, I. M. 1965 *Introduction to the Theory of Superfluidity*. Benjamin.

LANDAU, L. D. & LIFSHITZ, E. M. 1959 Fluid mechanics. In *Course of Theoretical Physics*. Pergamon.

LINK, B., EPSTEIN, R. I. & VAN RIPER, K. A. 1992 Pulsar glitches as probes of neutron star interiors. *Nature* **359**, 616–618.

LOPER, D. E. 1971 Hydromagnetic spin-up of a fluid confined by two flat electrically conducting boundaries. *J. Fluid Mech.* **50**, 609–623.

LYNE, A. G., SHEMAR, S. L. & SMITH, F. G. 2000 Statistical studies of pulsar glitches. *Mon. Not. R. Astron. Soc.* **315**, 534–542.

MELATOS, A., PERALTA, C. & WYITHE, J. S. B. 2008 Avalanche dynamics of radio pulsar glitches. *Astrophys. J.* **672**, 1103–1118.

MENDELL, G. 1991*a* Superfluid hydrodynamics in rotating neutron stars. Part 1. Nondissipative equations. *Astrophys. J.* **380**, 515–529.

MENDELL, G. 1991*b* Superfluid hydrodynamics in rotating neutron stars. Part 2. Dissipative effects. *Astrophys. J.* **380**, 530–540.

ONSAGER, L. 1931 Reciprocal relations in irreversible processes. Part 1. *Phys. Rev.* **37**, 405–426.

PAOLETTI, M. S. & LATHROP, D. P. 2011 Quantum turbulence. *Annu. Rev. Condens. Matter Phys.* **2**, 213–234.

PEDLOSKY, J. 1967 The spin up of a stratified fluid. *J. Fluid Mech.* **28**, 463–479.

PERADZYNSKI, Z., FILIPKOWSKI, S. & FISZDON, W. 1990 Spin-up of He II in a cylindrical vessel of finite height. *Eur. J. Mech.* B **9**, 259–272.

PERALTA, C., MELATOS, A., GIACOBELLO, M. & OOI, A. 2005 Global three-dimensional flow of a neutron superfluid in a spherical shell in a neutron star. *Astrophys. J.* **635**, 1224–1232.

PERALTA, C., MELATOS, A., GIACOBELLO, M. & OOI, A. 2006 Transitions between turbulent and laminar superfluid vorticity states in the outer core of a neutron star. *Astrophys. J.* **651**, 1079–1091.

https://doi.org/10.1017/jfm.2013.294 Published online by Cambridge University Press

PERALTA, C., MELATOS, A., GIACOBELLO, M. & OOI, A. 2008 Superfluid spherical Couette flow. *J. Fluid Mech.* **609**, 221–274.

REISENEGGER, A. 1993 The spin-up problem in Helium II. *J. Low Temp. Phys.* **92**, 77–106.

SKRBEK, L. & SREENIVASAN, K. R. 2012 Developed quantum turbulence and its decay. *Phys. Fluids* **24** (1), 011301.

TSAKADZE, J. S. & TSAKADZE, S. J. 1972 Relaxation phenomena at acceleration of rotation of a spherical vessel with helium II and relaxation in pulsars. *Phys. Lett.* A **41**, 197–199.

TSAKADZE, J. S. & TSAKADZE, S. J. 1973 Measurement of the relaxation time on acceleration of vessels with helium II and superfluidity in pulsars. *Sov. J. Expl Theoret. Phys.* **37**, 918–921.

TSAKADZE, J. S. & TSAKADZE, S. J. 1974 On the problem of relaxation time determination in superfluids when their rotation is accelerated. *Phys. Lett.* A **47**, 477–478.

TSAKADZE, J. S. & TSAKADZE, S. J. 1980 Properties of slowly rotating helium II and the superfluidity of pulsars. *J. Low Temp. Phys.* **39**, 649–688.

TSUBOTA, M. 2009 Quantum turbulence: from superfluid helium to atomic Bose–Einstein condensates. *J. Phys.: Condens. Matter* **21** (16), 164207.

TSUBOTA, M., BARENGHI, C. F., ARAKI, T. & MITANI, A. 2004 Instability of vortex array and transitions to turbulence in rotating helium II. *Phys. Rev.* B **69** (13), 134515.

UNGARISH, M. 1990 Spin-up from rest of a mixture. *Phys. Fluids* **2**, 160–166.

VAN EYSDEN, C. A. & MELATOS, A. 2008 Gravitational radiation from pulsar glitches. *Class. Quant. Grav.* **25** (22), 225020.

VAN EYSDEN, C. A. & MELATOS, A. 2010 Pulsar glitch recovery and the superfluidity coefficients of bulk nuclear matter. *Mon. Not. R. Astron. Soc.* **409**, 1253–1268.

VAN EYSDEN, C. A. & MELATOS, A. 2011 Spin down of superfluid-filled vessels: theory versus experiment. *J. Low Temp. Phys.* **165**, 1–14.

VAN EYSDEN, C. A. & MELATOS, A. 2012 Interpreting superfluid spin up through the response of the container. *J. Low Temp. Phys.* **166**, 151–170.

VINEN, W. F. 2010 Quantum turbulence: achievements and challenges. *J. Low Temp. Phys.* **161**, 419–444.

VINEN, W. F. & NIEMELA, J. J. 2002 Quantum turbulence. *J. Low Temp. Phys.* **128**, 167–231.

WALIN, G. 1969 Some aspects of time-dependent motion of a stratified rotating fluid. *J. Fluid Mech.* **36**, 289–307.

WALMSLEY, P. M., GOLOV, A. I., HALL, H. E., LEVCHENKO, A. A. & VINEN, W. F. 2007 Dissipation of quantum turbulence in the zero temperature limit. *Phys. Rev. Lett.* **99** (26), 265302.

WANG, N., MANCHESTER, R. N., PACE, R. T., BAILES, M., KASPI, V. M., STAPPERS, B. W. & LYNE, A. G. 2000 Glitches in southern pulsars. *Mon. Not. R. Astron. Soc.* **317**, 843–860.

WARSZAWSKI, L. & MELATOS, A. 2013 Knock-on processes in superfluid vortex avalanches and pulsar glitch statistics. *Mon. Not. R. Astron. Soc.* **428**, 1911–1926.

WARSZAWSKI, L., MELATOS, A. & BERLOFF, N. G. 2012 Unpinning triggers for superfluid vortex avalanches. *Phys. Rev.* B **85** (10), 104503.

WEDEMEYER, E. H. 1964 The unsteady flow within a spinning cylinder. *J. Fluid Mech.* **20**, 383–399.

ZWILLINGER, D. 1989 *Handbook of Differential Equations*. Academic.

https://doi.org/10.1017/jfm.2013.294 Published online by Cambridge University Press